Affine Invariants of Vector Fields

Jitka Kostková, Tomáš Suk, and Jan Flusser, *Senior Member, IEEE*

Abstract—Vector fields are a special kind of multidimensional data, which are in a certain sense similar to digital color images, but are distinct from them in several aspects. In each pixel, the field is assigned to a vector that shows the direction and the magnitude of the quantity, which has been measured. To detect the patterns of interest in the field, special matching methods must be developed. In this paper, we propose a method for the description and matching of vector field patterns under an unknown affine transformation of the field. Unlike digital images, transformations of vector fields act not only on the spatial coordinates but also on the field values, which makes the detection different from the image case. To measure the similarity between the template and the field patch, we propose original invariants with respect to total affine transformation. They are designed from the vector field moments. It is demonstrated by experiments on real data from fluid mechanics that they perform significantly better than potential competitors.

Index Terms—Vector field, total affine transformation, affine invariants, template matching, vector field moments

1 Introduction

Analysis of *vector fields* has been attracting an increasing attention in last ten years. Vector fields are special kind of multidimensional data, that appear in numerous scientific and engineering areas, such as in mechanical engineering, fluid dynamics, medicine, computer vision, and meteorology. They describe particle velocity, wind velocity, optical/motion flow, image gradient, and other phenomena.

In fluid mechanics, flow fields and their mathematical models (mostly based on Navier-Stokes equations) have been studied for centuries. However, in connection with new devices/techniques producing vector or even tensor field data, such as diffusion tensor imaging, the tasks appeared which seem to be better resolved by signal-processing approach rather than by traditional fluid mechanics.

A typical example of such task is the detection of various patterns of interest. It comprises not only detection of singularities such as vortices, saddle points, vortex-saddle combinations, and double vortices (these could be found by traditional techniques as well), but also detection of arbitrary patterns, which are similar to the patterns stored in the pattern-of-interest database (these patterns may be extracted from similar fields or obtained as a result of a simulation). Since the patterns of interest may not have any special mathematical properties, their detection by traditional tools is questionable or even impossible.

The detection of these patterns can be accomplished by *template matching*, which is a technique widely applied in image processing but relatively new in vector field analysis. The search algorithm evaluates the similarity between the template and a field patch and must be primarily *invariant* with respect to all possible pattern deformations, which might be present (for instance, the template stored in the database may depict a circular vortex, but we want to find also all elliptic vortices of arbitrary size and orientation, which may appear near obstacles and boundaries). Fig. 1 schematically shows the pattern matching in a vector field.

The main contribution of this paper is the derivation of a new class of vector-field invariants, which are suitable for template matching. We assume the template deformations can be modeled by so called *total affine transformation* (TAFT – see Section 2 for mathematical description). This assumption is realistic and the underlaying model is reasonably general, but still possible to be handled thanks to its linearity. This problem formulation is original and we are not aware of any other paper, which would come up with a formulation and/or a solution of a similar task. We also introduce *multilayer graphs*, which can represent the invariants and can be employed for their automatic generation and for studying their properties. Showing the connection between the invariants and the multilayer graphs is another significant theoretical contribution of the paper.

The paper is structured as follows. After giving a survey of relevant literature in Section 3, we introduce vector field invariants w.r.t. TAFT, composed of the moments of the field, in Section 4. In Section 5, we introduce the notion of a multi-layer graph and establish the connection between the invariants and the multi-layer graphs, which helps to understand the structure of the set of invariants. Section 6 presents algorithms for generating all graphs that represent the invariants. Since such set is highly redundant, we propose a selection of complete and independent set in Section 7. Finally, in Section 8 we demonstrate the performance and the advantages of these invariants in affine-invariant template matching on simulated and real data.

2 Vector Fields and their Transformations

In this section, we formally define a vector field, introduce the notion of its *total transformation* and show how the

• *The authors are with the Czech Academy of Sciences, Institute of Information Theory and Automation, Pod vodárenskou věží 4, Praha 8 182 08, Czech Republic. E-mail: {kostkova, suk, flusser}@utia.cas.cz.*

Manuscript received 31 Mar. 2018; revised 9 Aug. 2019; accepted 27 Oct. 2019. Date of publication 6 Nov. 2019; date of current version 4 Mar. 2021. (Corresponding author: Jan Flusser.)
Recommended for acceptance by B. Morse.
Digital Object Identifier no. 10.1109/TPAMI.2019.2951664

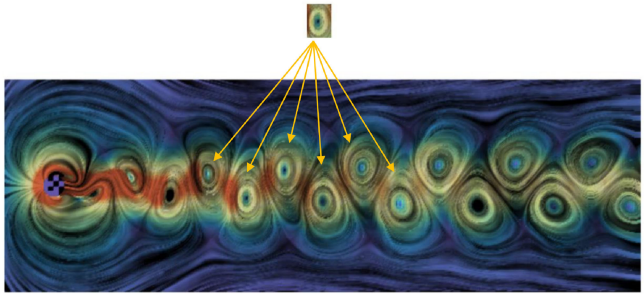

Fig. 1. Vortex detection in a swirling fluid by template matching. The detection method must be invariant to the template deformation.

transformations of "traditional" images and vector fields differ from one another, even if both can be understood as particular cases of total transformations.

Definition 1. *A 2D vector field* $\mathbf{f}(\mathbf{x})$ *is an ordered pair of scalar fields* $\mathbf{f}(\mathbf{x}) = (f_1(\mathbf{x}), f_2(\mathbf{x}))$.

At each point $\mathbf{x} = (\mathrm{x}, \mathrm{y})$, the value of $\mathbf{f}(\mathbf{x})$ shows the orientation and the magnitude of the measured vector. The scalar field $f_i(\mathbf{x})$ can be understood as a graylevel image which may contain also negative values.[1]

By a total transformation we understand any transformation in the vector field space, which acts simultaneously in spatial and function domains. Even if this definition can be used for arbitrary (non-linear) transformations, in this paper we restrict to linear ones.

Definition 2. *Let* A *and* B *be regular matrices and* $\mathbf{f}$ *be a vector field. The transformation* $\mathbf{f} \to \mathbf{f}'$*, where*

$$\mathbf{f}'(\mathbf{x}) = B\mathbf{f}(A^{-1}\mathbf{x}), \tag{1}$$

is called independent total affine transformation *of the field* $\mathbf{f}$*. Matrix* A *is called* inner *transformation matrix (or just inner transformation for short), while matrix* B *is called* outer *transformation matrix.*

The above transformation model does not contain a shift, which is basically for two reasons. The shift in the outer part might occur as a basic flow in the background and can be removed by subtracting the background flow from the entire field. The shift in the inner part, which is independent of the outer shift, may appear in some applications and captures the translation of the field in the plane. In such a case, $A^{-1}\mathbf{x}$ is replaced with $A^{-1}\mathbf{x} + \mathbf{t}$ in the model. However, for pattern detection via template matching it is irrelevant to include the shift into the deformation model, because the shift is the key parameter we want to detect. If, in some other applications, incorporating the shift was desirable, it would be sufficient to replace the moments in the invariants (see Section 4) with central moments related to a properly defined field centroid and we automatically obtain invariants to inner translation.

In reality, vector fields are mostly transformed by a slightly simpler transformation than (1) in which $A = B$. Such a model is called *special total affine transformation* and captures one of the basic properties of vector fields – if the field is transformed in the space domain, the function domain (i.e., the vector values) are transformed *by the same transformation*. The scenarios where $A \neq B$ are rare, but may happen as well if, for instance, the measuring device exhibits different calibrations for inner and outer part. The special transformation can be understood intuitively. Let us imagine the vector field as an array of arrows. If we deform spatially the array, the absolute orientation and length of the arrows must be changed accordingly such that their relative orientation and length is preserved (see Fig. 2 for an example).

This is the principal difference between "true" vector fields and images. Traditional images can be viewed as particular cases of vector fields, where the number of components equals the number of the spectral bands. Most often, they are transformed with $B = I$, where I is an identity matrix, and the transformation is purely spatial. The total transformation model can also capture the spatial transformation accompanied by contrast changes of individual channels (when B is diagonal different from I) or by spectral mixing (when B is not diagonal). However, the situations when B is not diagonal are rare for traditional images and in any case, there is absolutely no reason why B should be the same as A.

In the theory of invariants, it is well known that the set of all admissible transformations, with respect to which we want to design invariants, must form a *group* or at least a *semi-group* (see, for instance, [1] or [2] for explanation). In particular, the transformations must exhibit the *closure property*—the composition of two arbitrary transformations must be again a transformation within the given set. The set of all independent total affine transformations is closed under composition. To see this, consider two such transformations given by matrices $A_i, B_i; i = 1, 2$, which have been applied consecutively to a vector field. The result is equivalent to applying a single independent total affine transformations with matrices $A = A_2A_1$ and $B = B_2B_1$. The closure property is preserved, if we consider special total affine transformations only. Both transformations are invertible and contain a unit element (identity transformation). Hence, both sets are groups (but not Abelian groups as matrix multiplication is not commutative).

3 Literature Survey

Although affine invariants of vector fields have never been studied, we still found several inspiring papers that formed the background of our current work. They fall basically into two categories: papers on rotation invariants of vector fields and papers on affine invariants of scalar and color images.

The problem of finding vector field invariants to total rotation was raised for the first time relatively recently by Schlemmer et al. [3], who adapted the scalar moment invariants proposed by Mostafa and Psaltis [4] and Flusser [5], [6] and designed invariants composed of geometric complex moments of the field. Schlemmer et al. used these invariants to detect specific patterns in a turbulent swirling jet flow. Rotation invariants from geometric complex moments have found several applications. Liu and Ribeiro [7] used them, along with a local approximation of the vector field by a polynomial, to detect singularities on meteorological satellite images showing wind velocity. Basically the same kind of rotation

1. Apart from 2D vector fields, there exist also 3D vector fields, matrix fields, and tensor fields. The study of these more general fields is beyond the scope of this paper.

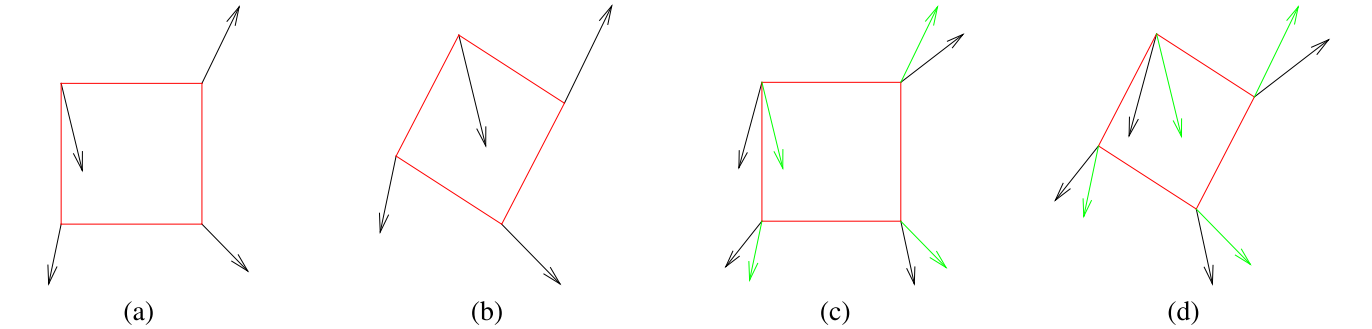

Fig. 2. Vector field transformations: (a) An original vector field, (b) its inner affine transformation, (c) its outer affine transformation, (d) its special total affine transformation. The green arrows in (c) and (d) show the vector field without the outer transformation.

invariants were used by Liu and Yap [8] for the indexing and recognition of fingerprint images. A generalization to more than two dimensions using tensor contraction was proposed by Langbein and Hagen [9]. Bujack et al. [10], [11] studied the invariants of complex moments thoroughly, generalized the previous works, and showed that the invariants can be derived also by means of the field normalization approach. Yang et al. improved the numerical stability of the invariants by using orthogonal Gaussian-Hermite [12] and Zernike [13] moments instead of the geometric ones. Most recently, Bujack [14] introduced so-called flexible basis of the invariants to avoid moments that vanish on the given templates. In all these papers, the authors considered the total rotation model only. The gap between total rotation and total affine transformation is so big that almost nothing from the referenced papers can be used or adapted to derive invariants w.r.t. total affine transformation.

Apart of the above methods, which all were more or less inspired by signal processing and approached a vector field as a specific multi-valued image, we can find several "non-image methods in flow analysis for detecting singularities. Comparing to the signal-based methods, they suffer from several limitations. The most serious one is that they were designed for detection of singularities only and cannot detect arbitrary templates. Majority of the existing methods concerns with the detection of vortices, other methods are able to detect foci, stable points or nodes. Vortex detection methods mostly compute the curl of the flow field, which characterizes vortices. Almost all methods for detection of other singularities calculate the gradient of the flow velocity and locally calculate the eigenvalues of the underlying tensor. The criterion "vortex/focus/node/..." is evaluated from these eigenvalues, differently in each individual method. They are not affine-invariant and cannot be easily generalized to this invariance, because intrinsically assume circular shape of the vortices. Some of those methods assume (at least implicitly) that the flow is ruled by Navier-Stokes equations. This is, however, not generally true for gradient fields and optical flow fields. Many methods of this kind can be found in the literature. A good survey of vorticity measures based on the determinant and trace of the flow velocity gradient tensor is given in [15], where the method of helicity [16], swirl parameter method [17], λ_2 method [18], Predictor-Corrector method [19], parallel vectors method [20], and streamline method [21] are reviewed and compared. Chen [22] describes various criteria (vorticity measures) for detection of vortices and their simplification in planar flow – Delta-criterion, λ_{ci} criterion, Q criterion, and λ_2 criterion (we use this method in the experimental section for comparison).

Comparing to the above group of papers on vector field rotation invariants, *affine moment invariants* (AMIs) of gray-level images have been studied in hundreds of papers and books in the last 100 years.[2] They can be traced back to the end of the 19th century, to the times when neither computers nor automatic object recognition existed. Probably the first one who systematically studied invariants to affine transformation was the famous German mathematician David Hilbert. He did not work explicitly with moments but studied so called *algebraic invariants* [23]. The algebraic invariants are polynomials of coefficients of a binary form, which are invariant w.r.t. an affine transformation. Hilbert had many followers, who elaborated the traditional theory of algebraic invariants in the late 19th and early 20th century, see for instance [24], [25], [26], [27], [28]. The algebraic invariants are closely linked with the AMIs through the *Fundamental theorem of the AMIs*, formulated (unfortunately incorrectly) by Hu [29] in 1962. Through this link, the core of the Hilbert's work can be adapted to moments in a relatively straightforward way. The Fundamental theorem of the AMIs was later corrected by Reiss [30] and Flusser and Suk [31]. Since then, several new methods of deriving AMIs have appeared. They differ from each other in the mathematical tools used. One may use graph theory as was proposed in [32], [33], tensor algebra [34], direct solution of proper partial differential equations [35], transvectants [36], and derivation via image normalization [37]. The resulting AMIs achieved by all these approaches are theoretically equivalent, because there exists a polynomial one-to-one mapping between any two AMI sets. However, differences can be found in complexity of the derivation and in numerical properties of the respective AMI's.

Special AMIs were proposed for color images [38], [39], [40], [41], [42], where the between-channel bond and various kinds of linear color changes were considered together with the spatial affine transformation.

4 Construction of VFAMIs

In this section, we propose *vector field moment invariants w.r.t. total affine transformation* (VFAMIs). The invariants, which we

2. There exist also many affine invariants, which are not based on moments, but they are irrelevant for this work, so we do not mention them here.

are going to construct, are functions of geometric moments of the field. In case of a 2D vector field **f** with the components f_1 and f_2 we may use standard geometric scalar moments [1], [2] given as

$$m_{pq}^{(i)} = \int_{-\infty}^{\infty}\int_{-\infty}^{\infty} x^p y^q f_i(x,y)\,\mathrm{d}x\,\mathrm{d}y\,. \tag{2}$$

Let us for simplicity assume that **f** is compactly supported and both f_i are piecewise continuous. Under these assumptions, all moments $m_{pq}^{(i)}$ of indices $p, q = 0, 1, 2, \ldots$ are well-defined and completely characterize the field **f**.

4.1 Invariants to Inner Transformation

Let us first construct the VFAMIs for the particular case of $B = I$ (this is essentially the problem of AMIs for two-band images). We start by constructing the AMIs for components f_1 and f_2 separately. To do so, we use the method proposed in [32] and further elaborated in [33], which guarantees to produce a complete set.

Let us consider two arbitrary points $\mathbf{x}_1 = (x_1, y_1)$, $\mathbf{x}_2 = (x_2, y_2)$ from the support of **f**. Let us denote the "cross-product" of these points as C_{12}

$$C_{12} = x_1 y_2 - x_2 y_1.$$

Geometric meaning of C_{12} is the oriented double area of the triangle, whose vertices are (x_1, y_1), (x_2, y_2), and (0, 0). After an affine transformation $\mathbf{x}' = A\mathbf{x}$ has been applied, the cross-product is transformed as $C'_{12} = J_A \cdot C_{12}$, where $J_A = \det(A)$ is the Jacobian of the transformation. This proves that C_{12} is a relative invariant with respect to inner transformation A. Now we consider various numbers of points (x_i, y_i) and we integrate their cross-products (or some integer powers of their cross-products) over the support of **f**. These integrals can be expressed in terms of moments and, after eliminating the Jacobian by a proper normalization, they yield absolute affine invariants.

More precisely, having $r > 1$ distinct points $(x_1, y_1), \ldots, (x_r, y_r)$, we define functional I of scalar f depending on r and on non-negative integers n_{kj} as

$$I(f) = \int_{-\infty}^{\infty}\cdots\int_{-\infty}^{\infty}\prod_{k,j=1}^{r} C_{kj}^{n_{kj}} \cdot \prod_{i=1}^{r} f(x_i, y_i)\,\mathrm{d}x_i\,\mathrm{d}y_i\,. \tag{3}$$

Note that it is meaningful to consider only $j > k$, because $C_{kj} = -C_{jk}$ and $C_{kk} = 0$.

After an inner affine transformation we have $f'(\mathbf{x}) = f(A^{-1}\mathbf{x})$ and $I(f')$ becomes

$$\begin{aligned} I(f') &= \int_{-\infty}^{\infty}\cdots\int_{-\infty}^{\infty}\prod_{k,j=1}^{r} C_{kj}^{n_{kj}} \cdot \prod_{i=1}^{r} f(A^{-1}\mathbf{x}_i)\,\mathrm{d}x_i\,\mathrm{d}y_i \\ &= \int_{-\infty}^{\infty}\cdots\int_{-\infty}^{\infty}\prod_{k,j=1}^{r} (C_{kj}^{n_{kj}})' \cdot \prod_{i=1}^{r} f(x_i, y_i)|J_A|^r\,\mathrm{d}x_i\,\mathrm{d}y_i \\ &= J_A^w |J_A|^r \cdot I(f)\,, \end{aligned} \tag{4}$$

where $w = \sum_{k,j} n_{kj}$ is the *weight* of the invariant and r is its *degree*. Hence, $I(f)$ is a relative affine invariant, too. If $I(f)$ is normalized by m_{00}^{w+r}, we obtain a desirable absolute affine invariant

$$\left(\frac{I(f)}{m_{00}^{w+r}}\right)' = \left(\frac{I(f)}{m_{00}^{w+r}}\right), \tag{5}$$

(if w is odd and $J < 0$ the sign change occurs in Eq. (5)). If we expand the integrand in Eq. (3) and integrate term-wise, we obtain an expression of I in terms of geometric moments of f. Varying r and n_{kj}, we can generate infinitely many invariants of all orders. Such a set is complete but highly redundant. The process of eliminating reducible invariants is described in [33].

The invariants from Eq. (5) can be derived separately for both field components f_1 and f_2. In addition to that, we can further employ the fact that transformation A is the same for both components, which brings a possibility of constructing *joint invariants* (i.e., those containing moments of both f_1 and f_2 at the same invariant). This idea was proposed in [38] in the context of invariants for color images and slightly increases the number of independent invariants.

For the sake of completeness, it should be mentioned that Eq. (3) may be formulated in a more general way as

$$I(f) = \int_{-\infty}^{\infty}\cdots\int_{-\infty}^{\infty}\prod_{k,j=1}^{r} C_{kj}^{n_{kj}} \cdot \prod_{i=1}^{r} f^{v_i}(x_i, y_i)\,\mathrm{d}x_i\,\mathrm{d}y_i\,, \tag{6}$$

where v_i are arbitrary powers. Eqs. (4) and (5) still hold (note that the normalization in (5) does not depend on v_i). However, the integration of (3) does not lead to moments of f but generally to moments of f^{v_i}. This is highly redundant, because the *moment uniqueness theorem* (see [2] for instance) assures that all moments of any f^{v_i} can be calculated from the moments of f. Hence, using $v_i \neq 1$ in (3) is generally useless and we do not follow that approach in this paper (it might be justifiable only if we confine ourselves to a few low moment orders, where the redundancy is weak, as for instance did the authors in [39], [40]).

4.2 Invariants to Outer Transformation

If $B \neq I$, it is not easy to extend the "inner" invariants from the previous section. The exception is when B is diagonal, so the components f_1 and f_2 are not mixed together. This is not realistic for "true" vector fields, but this model was studied in the connection with color images of indoor scenes, underlaying photometric transformation due to a varying illumination [43], [44]. If B is diagonal, the invariants (3) of the component f_i are just multiplied by B_{ii}^r. This multiplication factor can be eliminated by taking a ratio of two invariants of the same r or by a ratios of proper powers of two arbitrary invariants.

Now let us consider arbitrary regular B, but assume for simplicity that $A = I$, so only an outer transformation of the vector field is effective. We proceed analogously to the previous section. The role of C_{kj} has been taken over by "component cross-products" F_{kj}

$$F_{kj} = f_1(x_k, y_k) f_2(x_j, y_j) - f_1(x_j, y_j) f_2(x_k, y_k)\,.$$

F_{kj} is a relative invariant w.r.t. outer affine transformation as

$$F'_{kj} = J_B \cdot F_{kj}\,,$$

where $J_B = \det(B)$ (see Appendix A for the proof). The simplest moment invariants are given as

$$O_{pqst}(\mathbf{f}) = \int_{-\infty}^{\infty} \cdots \int_{-\infty}^{\infty} x_1^p y_1^q x_2^s y_2^t F_{12}\, \mathrm{d}x_1\, \mathrm{d}x_2\, \mathrm{d}y_1\, \mathrm{d}y_2\,, \tag{7}$$

which yields, after the term-wise integration, the moment form

$$O_{pqst}(\mathbf{f}) = m_{pq}^{(1)} m_{st}^{(2)} - m_{st}^{(1)} m_{pq}^{(2)}\,. \tag{8}$$

The relative invariance property $O_{pqst}(\mathbf{f}') = J_B \cdot O_{pqst}(\mathbf{f})$ follows immediately from the same of F_{12}. Eq. (8) yields a non-trivial invariant for arbitrary combinations of indices except $(p,q) = (s,t)$ (note that $O_{pqpq}(\mathbf{f}) = 0$ for any p, q, and $\mathbf{f}$). Swapping of the indices $(p,q) \leftrightarrow (s,t)$ just changes the sign as $O_{pqst}(\mathbf{f}) = -O_{stpq}(\mathbf{f})$ and does not yield an independent invariant. Hence, using all non-trivial configurations of indices p, q, s, t up to the given order R, we obtain $R(R+1)(R+2)(R+3)/8$ invariants of the form (8). Since there exist only $(R+1)(R+2)$ moments, it is clear that the set of invariants is redundant and must contain dependent invariants. Since the outer transformation has four degrees of freedom, the number of independent invariants is at most $(R+1)(R+2) - 4$. Although the number of the invariants (8)) is higher for any $R > 0$, it is not automatically guaranteed that they are complete.

To prove the completeness, we show that from the knowledge of all invariants of the form (8) we can recover all moment values, except four freely chosen moments the value of which may be arbitrary. Let us assume there exists at least one invariant such that $O_{pqst} \neq 0$ (if this is not the case, then $f_1 = \alpha f_2$, all invariants (8) vanish, and $\mathbf{f}$ is called a *coupled field*). Choose indices a, b arbitrary such that $(a,b) \neq (p,q)$ and $(a,b) \neq (s,t)$ and solve the system

$$\begin{aligned} m_{pq}^{(2)} m_{ab}^{(1)} - m_{pq}^{(1)} m_{ab}^{(2)} &= O_{abpq} \\ m_{st}^{(2)} m_{ab}^{(1)} - m_{st}^{(1)} m_{ab}^{(2)} &= O_{abst}, \end{aligned} \tag{9}$$

for $m_{ab}^{(1)}$ and $m_{ab}^{(2)}$. The determinant of the system equals O_{pqst}, which means the system is regular and unambiguously solvable, regardless of particular values of $m_{pq}^{(1)}, m_{pq}^{(2)}$, $m_{st}^{(1)}$, and $m_{st}^{(2)}$, which may be chosen freely. Keeping their choice fixed, this process is repeated for all admissible couples (a,b). In this way we recover all moments of the field from its invariants, up to the four degrees of freedom due to the transformation matrix B.

Invariants to outer transformation of a field can also be obtained in a general form analogous to Eq. (6) as

$$O(f) = \int_{-\infty}^{\infty} \cdots \int_{-\infty}^{\infty} \prod_{k,j=1}^{r} F_{kj}^{v_{kj}} \cdot \prod_{i=1}^{r} x_i^{p_i} y_i^{q_i}\, \mathrm{d}x_i\, \mathrm{d}y_i\,, \tag{10}$$

which leads to relative invariants given by

$$O(\mathbf{f}') = J_B^v \cdot O(\mathbf{f})\,,$$

where $v = \sum v_{kj}$. However, in the case of pure outer transformation this is useless. Since Eq. (8) generates a complete set of invariants by itself, any additional invariant designed by Eq. (10) is a function of them and does not carry any independent information.

Summarizing this section, we proved that Eq. (8) constitutes relative invariants w.r.t. outer transformation of a vector field. We proved they form a complete system. Absolute invariants are obtained as a ratio of any two non-trivial relative invariants (8). We also showed that the only vector fields laying in the joint null-space of the invariants are coupled fields, which must be handled separately and described by other invariants.

4.3 Invariants to Total Transformation

In this section, we go to the core of the problem. We show how to put the inner and outer invariants together and we propose vector field invariants w.r.t. total affine transformation. The key definition, analogous to (6) and (10), is now

$$V(\mathbf{f}) = \int_{-\infty}^{\infty} \cdots \int_{-\infty}^{\infty} \prod_{k,j=1}^{r} C_{kj}^{n_{kj}} \cdot F_{kj}^{v_{kj}} \cdot \prod_{i=1}^{r} \mathrm{d}x_i\, \mathrm{d}y_i\,. \tag{11}$$

$V(\mathbf{f})$ is a relative invariant as

$$V(\mathbf{f}') = J_B^v J_A^w |J_A|^r V(\mathbf{f})\,. \tag{12}$$

To eliminate J_A and J_B and obtain an absolute invariant, we have to normalize the relative invariant (11) by proper powers of other two relative invariants such that both Jacobians get canceled.[3]

If used extensively with many various parameters, Eq. (11) yields a huge number of redundant invariants. The first step to eliminate the redundancy is to fulfill the constraint that $V(\mathbf{f})$ must be composed solely of moments of the field $\mathbf{f}$. This is equivalent to the constraints imposed on the powers v_{kj}. Considering all possible index pairs (k,j), each of the points $(x_1, y_1), \ldots, (x_r, y_r)$ must be involved just once in all F_{kj}'s used. Hence, any v_{kj} can only equal 0 or 1, $v = r/2$ (which immediately implies that r must be even), and $v_{kj} = 0$ for all $k \geq j$ (this constraint is because $F_{kj} = -F_{jk}$ and $F_{kk} = 0$, so it would be useless to include them into the invariant). If $v_{kj} = 1$, then $v_{mj} = v_{jm} = v_{km} = v_{mk} = 0$ for all index pairs different from (k,j).

We may notice, that generating VFAMIs from Eq. (11), even if the choice of v_{kj} has been constrained as mentioned above, leads to many invariants, which are identically zero or which are somehow dependent on the other invariants that have been obtained from Eq. (11)) with other settings of the parameters. For instance, the simplest ever choice of $r = 2, v_{12} = 1$ and $n_{12} = 0$ yields a vanishing invariant; the same is true for $r = 2, v_{12} = 1, n_{12} = 2$ and for many other choices with higher r (the setting of $r = 4, v_{14} = v_{23} = 1$ and $n_{12} = n_{13} = n_{24} = n_{34} = 1, n_{kj} = 0$ otherwise, is an example leading to another vanishing invariant). As an example of a simple dependency, we may choose $r = 4, v_{12} = v_{34} = 1, n_{12} = n_{34} = 1, n_{kj} = 0$ otherwise, which leads to invariant $V(\mathbf{f}) = V_a^2$. Another example is the setting $r = 4, v_{12} = v_{34} = 1, n_{12} = 3, n_{34} = 1, n_{kj} = 0$ otherwise, which yields $V(\mathbf{f}) = V_a V_b$ (see below for explicit forms of V_a and V_b). Dependent invariants do not contribute to the recognition power of the system and only increase the dimensionality of the invariant set. It is highly desirable to identify them and exclude them from the set. An algorithm for detection of dependent invariants is proposed in Section 7.

3. Unlike scalar AMIs, we cannot normalize by a power of m_{00} because m_{00} is not a relative invariant w.r.t. the total affine transformation.

As an example, we show four simple VFAMIs in explicit forms below; hundreds of other invariants generated from Eq. (11) can be found on our webpage zoi.utia.cas.cz/affine-vector-fields.

The simplest non-trivial choice is $r = 2$ and $n_{12} = v_{12} = 1$, which yields

$$V_a = m_{10}^{(1)} m_{01}^{(2)} - m_{10}^{(2)} m_{01}^{(1)} .$$

The choice of $r = 2, v_{12} = 1$ and $n_{12} = 3$ yields

$$V_b = m_{30}^{(1)} m_{03}^{(2)} - 3m_{21}^{(1)} m_{12}^{(2)} + 3m_{12}^{(1)} m_{21}^{(2)} - m_{03}^{(1)} m_{30}^{(2)} .$$

The parameters $r = 2$, $v_{12} = 1$ and $n_{12} = 5$ lead to the invariant

$$\begin{aligned} V_c = {} & m_{50}^{(1)} m_{05}^{(2)} - 5m_{41}^{(1)} m_{14}^{(2)} + 10m_{32}^{(1)} m_{23}^{(2)} - 10m_{23}^{(1)} m_{32}^{(2)} \\ & + 5m_{14}^{(1)} m_{41}^{(2)} - m_{05}^{(1)} m_{50}^{(2)} . \end{aligned}$$

If we choose $r = 4$, $v_{12} = v_{34} = 1$ and $n_{12} = n_{13} = n_{24} = n_{34} = 1$, $n_{kj} = 0$ otherwise, we obtain

$$\begin{aligned} V_d = {} & -(m_{20}^{(1)})^2 (m_{02}^{(2)})^2 + 4m_{20}^{(1)} m_{11}^{(1)} m_{11}^{(2)} m_{02}^{(2)} \\ & + 2m_{20}^{(1)} m_{02}^{(1)} m_{20}^{(2)} m_{02}^{(2)} - 4m_{20}^{(1)} m_{02}^{(1)} (m_{11}^{(2)})^2 \\ & - 4(m_{11}^{(1)})^2 m_{20}^{(2)} m_{02}^{(2)} + 4m_{11}^{(1)} m_{02}^{(1)} m_{20}^{(2)} m_{11}^{(2)} \\ & - (m_{02}^{(1)})^2 (m_{20}^{(2)})^2 . \end{aligned}$$

If the vector field in question is a coupled field, all invariants generated from Eq. (11) obviously vanish. In such a case, we use only the first component of the field and treat it as a scalar image undergoing spatial affine transformation and contrast stretching. Any ratio of absolute scalar AMIs (5) of the same degree r and weight w yields a desired invariant.

4.4 Invariants to Special Total Transformation

As we already explained, the inner and outer transformations of a vector field are often the same, i.e., $A = B$ and Eq. (12) is simplified to the form

$$V(\mathbf{f}') = J_A^{w+r/2} |J_A|^r V(\mathbf{f}) . \tag{13}$$

The normalization can be accomplished just by one invariant, while the other one, which was needed to cancel J_B before, can be saved for recognition. This is, however, not the only difference. Since the number of degrees of freedom of the transformation has been reduced from eight to four, one may expect the existence of four additional independent invariants.

For a special total transformation, there exists yet another possibility how to generate invariants. We can replace the "intensity cross-product" F_{kj} by the "mixed cross-product"

$$D_{kj} = y_j f_1(x_k, y_k) - x_j f_2(x_k, y_k) .$$

D_{kj} is a relative invariant w.r.t. special total transformation as

$$D'_{kj} = J_A \cdot D_{kj}.$$

(see Appendix B for the proof). Unlike the previous case, here generally D_{kj} and D_{jk} are independent, and $D_{kk} \neq 0$.

Similarly to Eq. (11), we define functional

$$W(\mathbf{f}) = \int_{-\infty}^{\infty} \cdots \int_{-\infty}^{\infty} \prod_{k,j=1}^{r} C_{kj}^{n_{kj}} \cdot D_{kj}^{u_{kj}} \cdot \prod_{i=1}^{r} \mathrm{d}x_i \, \mathrm{d}y_i , \tag{14}$$

which is a relative invariant because

$$W(\mathbf{f}') = J_A^{w+u} |J_A|^r W(\mathbf{f}) . \tag{15}$$

Eq. (14) leads to moments only under certain restrictions, imposed on exponents u_{kj}. Each of the points $(x_1, y_1), \ldots, (x_r, y_r)$ must be involved just once as a field argument in all D_{kj}'s used. Hence, any u_{kj} can only equal 0 or 1 and $u \equiv \sum u_{kj} = r$.

We may go even further and generate invariants of the form

$$Z(\mathbf{f}) = \int_{-\infty}^{\infty} \cdots \int_{-\infty}^{\infty} \prod_{k,j=1}^{r} C_{kj}^{n_{kj}} \cdot F_{kj}^{v_{kj}} \cdot D_{kj}^{u_{kj}} \cdot \prod_{i=1}^{r} \mathrm{d}x_i \, \mathrm{d}y_i . \tag{16}$$

In this case, however, the constraints on v and u are different from the previous cases and are linked together. It still holds that each point (x_i, y_i) must appear just once as a field argument in the integrand. Hence, $2v + u = r$. Any v_{kj} and u_{kj} can only equal 0 or 1 as before, but they are further constrained as follows. If $v_{kj} = 1$, then $v_{mj} = v_{jm} = v_{km} = v_{mk} = 0$ for all index pairs except (k, j) and $u_{km} = u_{jm} = 0$ for any m. If $u_{kj} = 1$, then $u_{km} = 0$ for any $m \neq j$ and $v_{km} = v_{mk} = 0$ for any m.

Z is again a relative invariant, since

$$Z(\mathbf{f}') = J_A^{w+v+u} |J_A|^r Z(\mathbf{f}) . \tag{17}$$

It should be, however, noted, that each of the sets generated by Eqs. (11), (14), and (16) is highly redundant even on its own, and this redundancy increases, if two or all three sets are used together. Actually, the invariants obtained from Eqs. (11) and (14) are nothing but a subset of those obtained from Eq. (16). Careful selection of independent (or at least irreducible) invariants is highly recommended for practical applications. Section 7 presents a selection algorithm.

5 VFAMIs and Multi-Layer Graphs

In this section, we establish the correspondence between VFAMIs generated by Eqs. (11), (14) and (16) and *multi-layer graphs*. The representation by multi-layer graphs helps to understand the structure of the VFAMIs and is also useful for elimination of reducible invariants. We start with the definition of multi-layer graphs.

Definition 3. *Let $\mathcal{V}$ be a set of vertices (nodes) and $E_1, E_2, \ldots, E_m$ be sets of edges. An ordered $(m+1)$-tuple $G = (\mathcal{V}; E_1, E_2, \ldots, E_m)$ is called a* multi-layer graph *on $\mathcal{V}$. Graph $G_k = (\mathcal{V}; E_k)$ is called the* kth layer *of graph G. If $m = 2$, G is called a* bi-layer graph. *If there exists a layer G_k, which is a multigraph (i.e., which contains multiple edges), then G is called* multi-layer multigraph.

Definition 4. *Let $G = (\mathcal{V}; E_1, E_2, \ldots, E_m)$ be a multi-layer (multi)graph. Ordinary (multi)graph $U_G = (\mathcal{V}; E_1 \cup E_2 \cup \cdots \cup E_m)$ is called a* union *of G. G is called* connected multi-layer graph *if U_G is a connected graph.*

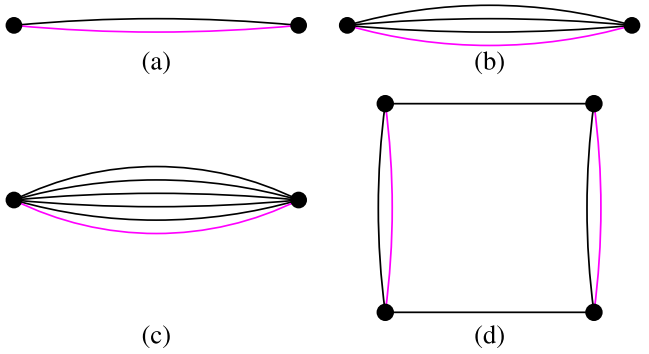

Fig. 3. The graphs representing invariants V_a, V_b, V_c, and V_d. The edges belonging to E_1 are shown in black, magenta edges belong to E_2.

Multi-layer graphs serve in many areas for modelling different network layers on the same set of nodes. The edges of different layers may be totally independent or there may be a kind of band among them.

An arbitrary invariant generated by Eq. (11) can be represented by a bi-layer graph as follows. Each point (x_k, y_k) corresponds to a graph node, so we have r nodes. Each cross-product C_{kj} corresponds to n_{kj} edges of the first layer connecting the kth and jth nodes (generally, the first layer is a multigraph). The second layer is constructed in a similar way—each intensity cross-product F_{kj} corresponds to v_{kj} edges (note that v_{kj} can only be zero or one). In Fig. 3, we can see the graphs representing invariants V_a, V_b, V_c, and V_d from Section 4.3. More examples of representation graphs can be found in Appendix C.

We can immediately make several simple statements about the bi-layer graphs than represent VFAMIs from Eq. (11).

1) The number of nodes is even.
2) In G_2, all nodes have degree one. If $r > 2$, then G_2 is not a connected graph.
3) Neither layer is a directed graph.
4) Neither layer contains self-loops.
5) If G is not connected, then the corresponding invariant is a product of several simpler invariants, which correspond to each connected component of G.
6) Any invariant of the form (11) is in fact a sum, where each term is a product of r moments. The order of the moments is preserved in all terms (for instance in V_4, there are always four moments of the second order in each term). The moment orders contained in a single term are the same as the degrees of all vertices in G_1.

The proof of all above statements follows immediately from Eq. (11) and from the definition of the corresponding graphs. We can see that the problem of generating all invariants is equivalent to finding all connected bi-layer graphs, satisfying the constraints 1–4.

Now let us assume the affine transformation is special one and consider the mixed invariants generated by Eq. (16). They can be represented by *three-layer graphs*, where the first two layers correspond to cross-products C_{kj} and F_{kj}, respectively, as before. The third layer G_3 corresponds to mixed cross-products D_{kj}. G_3 is a *directed* graph because D_{kj} and D_{jk} are different and we have to distinguish between them. We define the "direction" of the edge corresponding to D_{kj} as from (x_k, y_k) to (x_j, y_j). It is easy to prove the following simple statements, they follow from Eq. (16) and from the way how the graph has been constructed.

1) The number of nodes may be arbitrary.
2) G_3 may contain loops, self-loops and double edges (with reverse direction).
3) In G_3, we define the *outdegree* of the vertex as the number of "tail" edge ends adjacent to this vertex. The *indegree* is the number of "head" edge ends adjacent to the vertex. The outdegree of any vertex is less or equal one. The indegree of any vertex may be arbitrary from zero to u.
4) Consider graph $(\mathcal{V}; E_2 \cup E_3)$. For each vertex, the sum of its degree in E_2 and its outdegree in E_3 is called the *cumulative degree*. The cumulative degree always equals one.
5) If there are two or more edges in E_2, then $(\mathcal{V}; E_2 \cup E_3)$ is not a connected graph. If there is one or no edge in E_2, then $(\mathcal{V}; E_2 \cup E_3)$ may or may not be connected.

Examples of representation graphs of this kind can be found in Appendix D.

The established correspondence between the invariants and the graphs can be efficiently used to generate the invariants. Instead of working directly with Eqs. (11) and (16) all trying all possible point pairs and parameter combinations, it is sufficient to generate all multi-layer graphs satisfying the constraints presented above. In the next section, we present an algorithm for a systematic graph generation.

6 Generating the Representation Multi-Layer Graphs

The algorithms for generating the graphs, which represent invariants V_i (11) and Z_i (16) are similar in main principles and differ from one another in details (yet important ones) only. We start with an algorithm that generates invariants V_i (11).

The task is to generate all bi-layer graphs satisfying the constraints. Each layer is generated separately. The graph nodes are numbered from 1 to r. The main idea is to begin with a graph that have the node labels as low as possible and then successively increase the node labels until the last possible graph has been reached.

To generate all possible first layers with w edges, we start with the graph on two nodes with a w-multiple edge connecting them. Matrix representation of such graph is

$$\begin{pmatrix} 1 & 1 & \dots & 1 & 1 \\ 2 & 2 & \dots & 2 & 2 \end{pmatrix}, \tag{18}$$

where the column $\begin{matrix} 1 \\ 2 \end{matrix}$ means an edge connecting the nodes 1 and 2. The "last" graph, on which the algorithm should stop, is

$$\begin{pmatrix} 1 & 2 & 3 & 4 & \dots & w-2 & w-1 & w-1 \\ 2 & 3 & 4 & 5 & \dots & w-1 & w & w \end{pmatrix}. \tag{19}$$

Starting from the first graph, we iterate the algorithm shown in Fig. 4.

To generate the second layer, we proceed analogically with some modifications. The first graph is now

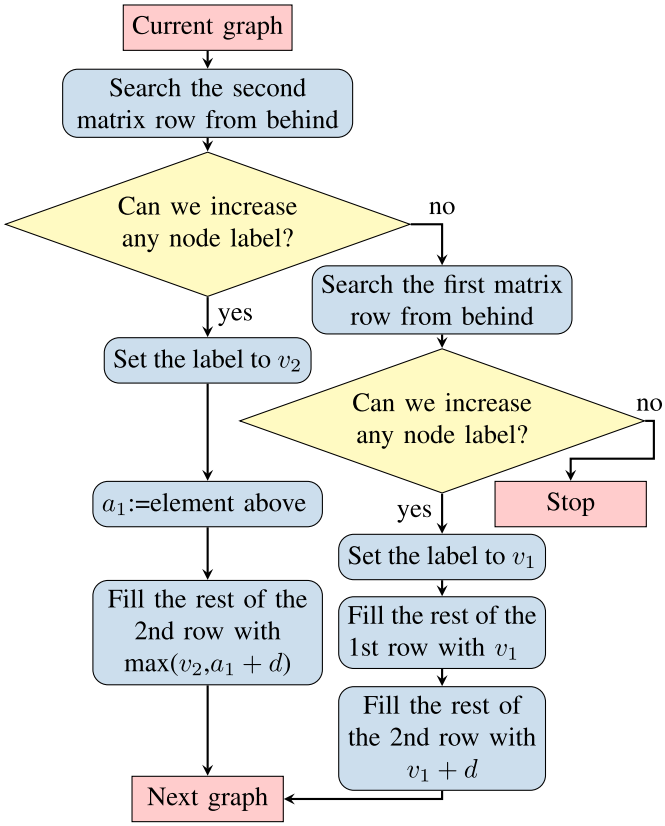

Fig. 4. Algorithm for the next graph generation. $d = 1$ for invariants V_i and $d = 0$ for invariants Z_i.

$$\begin{pmatrix} 1 & 3 & \dots & r-3 & r-1 \\ 2 & 4 & \dots & r-2 & r \end{pmatrix}. \tag{20}$$

As we already explained, r must be even and the representation matrix has $r/2$ columns. The inner loop of the algorithm must be modified, too. The criterion, if a matrix element can be increased, is not its comparison with the final graph, but the test, if there is a non-used node.

1) Set k to $r-1$, it is the last but one edge.
2) Test the second node of the kth edge. If there is a node with higher label, set it; otherwise decrease k by one.
3) If k is zero, no other graph can be generated. Stop.
4) Assign the free nodes to the edges behind k.
5) got to 2).

The generating algorithm of Z_i is in principle analogical to the previous one. Modifications are required when generating E_3 edges because the third layer is a directed graph, self-loops are allowed and there is a strong constraint on a cumulative $E_2 - E_3$ degree of each vertex. Since these modifications are rather technical ones, we do not describe this algorithm in detail.

A complete description of the algorithms for generating of both V_i and Z_i, including commented codes, can be found on http://zoi.utia.cas.cz/affine-vector-fields. On the same website, the reader may find extensive collections of the invariants (explicit formulas along with the representation graphs) – 6,323 invariants of type Z_i and 1,890 invariants of type V_i. On http://zoi.utia.cas.cz/Afintensors, we made available the software by means of which these invariants were generated. The software is in C++, has a user-friendly GUI and a detailed manual, so the readers may generate their own collections of the invariants with various parameters.

7 Selection of a Complete and Independent Set of the Invariants

In an ideal case, any feature set for object recognition should be complete and independent. The completeness means that the object can be precisely reconstructed (modulo the intra-class transformation group) from the values of the invariants and guarantees the maximum possible discrimination power. The independence ensures that the invariants do not contain any redundant information. The features are called dependent, if some of them is a function of the others; otherwise they are independent. While the independence is always desirable to keep the feature space dimensionality low, the completeness may not be necessary. In most practical cases, the objects in question can be discriminated from each other by a small incomplete subset.

Both the invariants V_i (11) and Z_i (16) form theoretically complete sets, if all possible parameter settings have been used. In reality, when the invariants are generated by the algorithms described in the previous section, we are always limited by the maximum number of edges w and that of nodes r, which leads to an incomplete set. This is, however, not a principal problem in practice. For any given database of sampled and quantized objects, we can find finite w and r such that the objects are distinguishable.

If used extensively, the algorithm generates a huge number of dependent invariants. We distinguish two kinds of dependencies among the invariants. The "simple" ones, which comprise linear combinations and products, can be found in the same way as in the case of graylevel AMIs (see [2], Chapter 5). The main idea is that a linear dependency may occur among invariants, whose representation graphs have the same numbers of nodes and the same numbers of edges going from individual nodes. We assemble a matrix of coefficients of all invariants generated by these graphs; the dependent invariants can be identified by singular value decomposition of this matrix. The eliminated invariants are called *reducible*, the remaining linearly and product independent invariants are called *irreducible*.

After the reducible invariants have been eliminated, there may still be polynomial dependencies among remaining invariants. The only method, which guarantees identifying all these dependencies is a kind of full search, but it is not computationally feasible. Instead, we propose two heuristics. No one guarantees to find all polynomial dependencies, but both are close to this optimum.

The first heuristics is based on the idea that the number of independent invariants n_i should equal the number of independent variables (moments) n_m minus the number of free parameters of the transformation group n_p (which is 8 for invariants V_i (11) and 4 for Z_i (16), if no translation is considered; otherwise it increases by two). We can take the generated irreducible invariants order by order, calculate the number n_i for each order separately and throw away all the invariants above this number. This method is very fast. As the result, we get the correct number of invariants, but there still might exist polynomial dependencies among them.

The second method is inspired by [36], it can also be found in [9]. If we have a dependent set of n_k invariants, there must exist function F such that

$$F(I_1, I_2, \ldots, I_{n_k}) = 0\,. \tag{21}$$

It must hold, for its derivatives with respect to an arbitrary moment (the proof is in [45])

$$\frac{\partial F(I_1, I_2, \ldots, I_{n_k})}{\partial m_{pq}^{(s)}} = 0\,. \tag{22}$$

Let us sort somehow the moments $m_{pq}^{(s)}$ and change their labels to m_j, where $j = 1, 2, \ldots, n_m$. We can decompose Eq. (22) to the form

$$\frac{\partial F(I_1, I_2, \ldots, I_{n_k})}{\partial m_j} = \sum_{\ell=1}^{n_k} \frac{\partial F(I_1, I_2, \ldots, I_{n_k})}{\partial I_\ell} \frac{\partial I_\ell}{\partial m_j} = 0\,, \tag{23}$$

where again $j = 1, 2, \ldots, n_m$.

The invariants as the functions of the moments are known, so the factor $\dfrac{\partial I_\ell}{\partial m_j}$ can be evaluated for specific values of the moments. The factor $\dfrac{\partial F(I_1, I_2, \ldots, I_{n_k})}{\partial I_\ell}$ is unknown, but it is the same for all j, it depends only on ℓ. Eq. (23) can be understood as a system of linear equations with the matrix of elements $a_{j\ell} = \dfrac{\partial I_\ell}{\partial m_j}$ of size $n_k \times n_m$ and the vector of unknown coefficients $b_\ell = \dfrac{\partial F(I_1, I_2, \ldots, I_{n_k})}{\partial I_\ell}$ of the size n_k. If the invariants are independent, the system can only have one solution with $b_\ell = 0$ for all ℓ. Then the matrix $(a_{j\ell})$ must have full rank n_k (it also means $n_k \leq n_m$). If the rank n_r is less than n_k, then only n_r invariants are independent (in this case n_k can be greater than n_m).

The above idea is clear and correct. However, when implementing it, we encounter some problems in computing the rank n_r of matrix $(a_{j\ell})$. It cannot be determined by symbolic computation. We should calculate $(a_{j\ell})$ on a representative set of objects and set n_r as the maximum particular rank. This would be impractical and time-consuming. Instead, we generate randomly five sets of moment values[4] and calculate the rank of the matrices via SVD using the Matlab in-built function `rank`. Then we estimate n_r as the maximum of these five particular ranks.

If we end up with $n_r \ll n_k$, we must somehow select n_r invariants out of n_k such that they are independent. We apply a sequential incremental procedure. First, we select the simplest invariant available. As soon as a subset of invariants has been selected, we add a new one such that the rank of $(a_{j\ell})$ increases by one. We iterate this process until the number n_r of the chosen invariants has been reached. Theoretically, this algorithm may select a dependent set due to the nesting effect. To improve it, we could implement a kind of backtracking, but this is actually a borderline problem that need not be solved in this case.

As we already pointed out, the graph generation algorithm is limited by the maximum number of edges. We run it for $w = 9$ at most. After eliminating the reducible invariants, we obtained 1,890 irreducible invariants of the type (11) and 6,323 irreducible invariants of the type (16) in explicit form. The selection algorithm based on the rank of $(a_{j\ell})$ yielded 76 and 77 independent invariants, respectively. They are listed on http://zoi.utia.cas.cz/affine-vector-fields. This process took 50 hours on a computer with the processor Intel Core i7-2600K CPU 3.4 GHz and 16 GB operational memory. It might seem too long, but note that this process is applied only once and does not depend on any data. As soon as the invariant sets have been created, we can apply them to any vector field without the necessity of their re-generation.

8 Numerical Experiments

8.1 Verification of the Invariance

In the first experiment, we verified the invariance property under simulated conditions. We transformed a vector field (which had been obtained as a gradient field of a grayscale Lena image, see Fig. 5) by 100 randomly generated independent TAFTs (i.e., transformations of the type (1), where A and B were independent) and calculated five invariants of V-type and five ones of Z-type. Theoretically, all V_k should be exactly invariant, while some Z_k may change since they are generally not invariant. The experiment confirmed this expectation (see Fig. 6 for visualization of the results). The small fluctuations of the V_k values appear due to the field resampling and interpolation, while the fluctuations of the Z_k values are really significant. If we constrain the transformation such that $B = A$, invariants Z_k become really invariant, as can be seen in Fig. 6c.

When we relaxed the perfect conditions, the invariance property became violated, but still the invariants exhibit a good robustness. We repeated the previous experiment, but we had added Gaussian noise independently to both field components before the field was transformed. We can observe the behavior of one selected invariant in Fig. 7, the others behave similarly. If SNR > 10 dB, the relative error is under 5 percent, which is fully acceptable.

8.2 Template Matching in a Gradient Field

In this experiment, we demonstrate the performance in template matching, for the present again in a controlled environment to be able to evaluate the results quantitatively. We calculated a gradient field of a real photograph and randomly selected 100 circular templates (see Fig. 8), the coordinates of which were drawn from a uniform distribution. Then we transformed the gradient field by a TAFT transformation and tried to localize the templates in the deformed field.

The matching was implemented as a search of all possible template locations and the matching position is determined as that one which minimizes ℓ_2-distance in the space of 33 invariants. If the localization error was less or equal than two pixels, the match was considered correct, and false otherwise.

We run this experiment ten times for various deformations and various template sets. The success rate in each run depends on the significance (structure) of the selected templates and also on the particular deformation. It ranged from 100 to 75 percent, being almost uniformly distributed between 95 and 80 percent. For a comparison, we applied in

4. Moment values of a vector field could be almost arbitrary, the only constraint is so-called complete monotonicity [2].

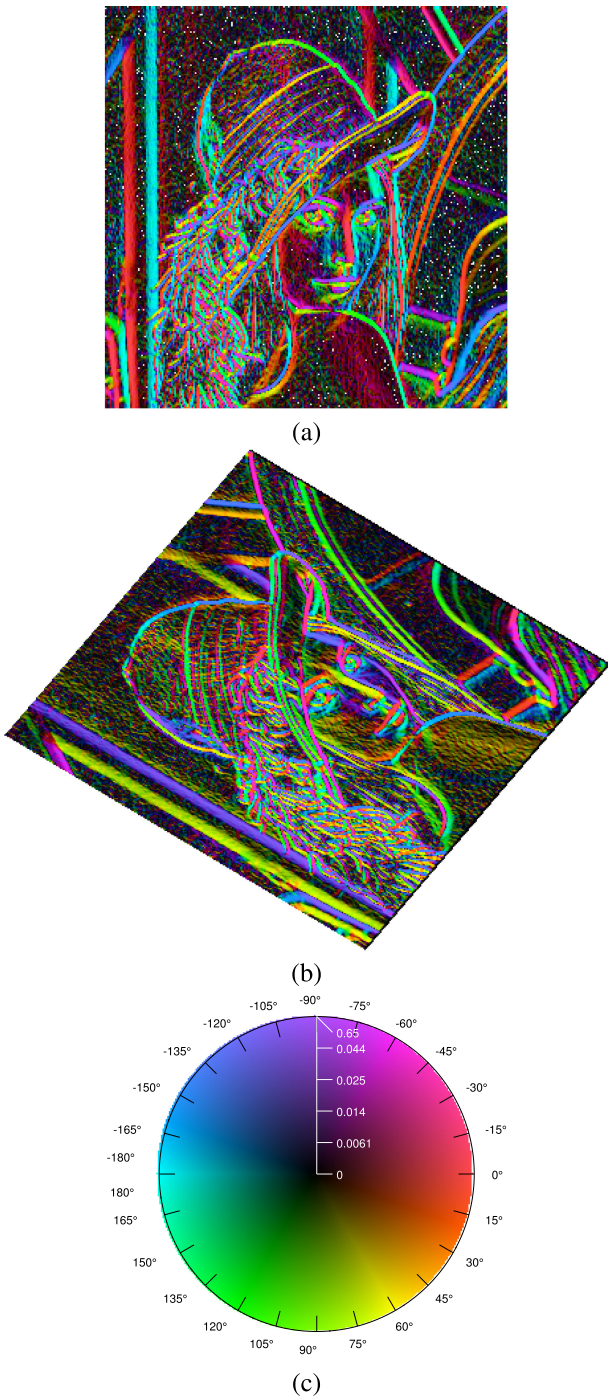

Fig. 5. (a) Gradient field of a grayscale image, which served as a test vector field in the synthetic experiments, (b) an example of the vector field transformed by a randomly generated TAFT, (c) colormap for gradient visualization, where the brightness corresponds to the magnitude and the hue to the direction of the gradient.

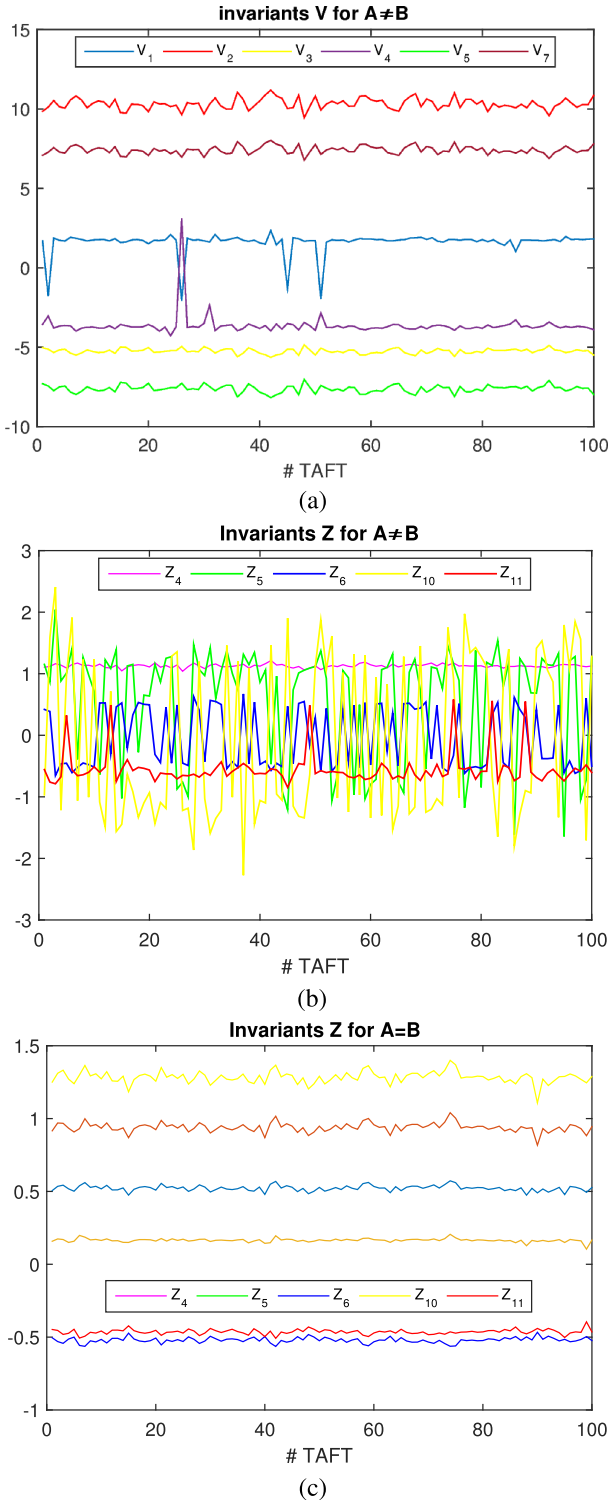

Fig. 6. The values of the invariants over 100 randomly generated total affine transformations. (a) Five selected invariants of the V-type exhibit very good invariance (except a few cases when the transformation is close to singular). (b) Invariants of the Z-type are not really invariant under these conditions. (c) The same invariants of the Z-type when the transformations were constrained such that $B = A$.

each run also rotation vector field invariants from [13]. Their success rate never exceeded 10 percent, which clearly illustrates the advantage of the affine invariants over the rotational ones if a true affine deformation is present.

8.3 Template Matching in a Fluid Flow Field

In this experiment, we demonstrate the applicability of the proposed invariants in an important problem from fluid dynamics engineering—vortex detection in a fluid flow vector field. We used the field showing the Kármán vortex street, which is a repeating pattern of swirling vortices caused by the flow of a fluid around blunt bodies. In the Kármán pattern, we can see several vortices arranged into two rows. The orientation of the "street" is given by the main flow direction and is generally not known a priori.

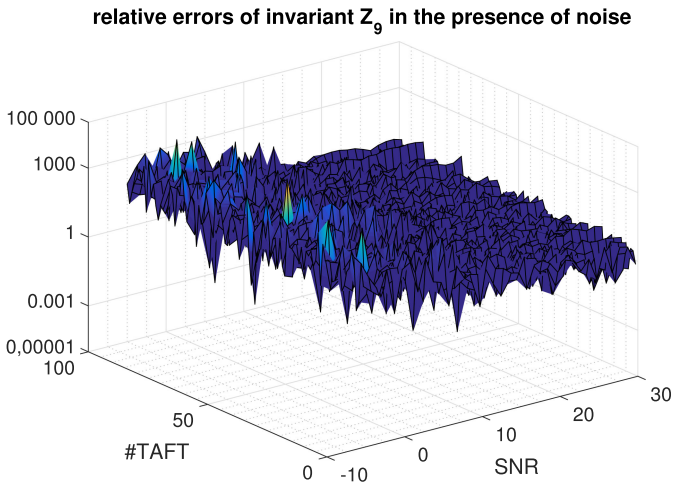

Fig. 7. The relative error of the invariant Z_9 over 100 randomly generated total affine transformations and SNR ranging from 30 to -5 dB. The robustness is very good for SNR > 10 dB. Only the ratio of the "noisy" and original value is visualized.

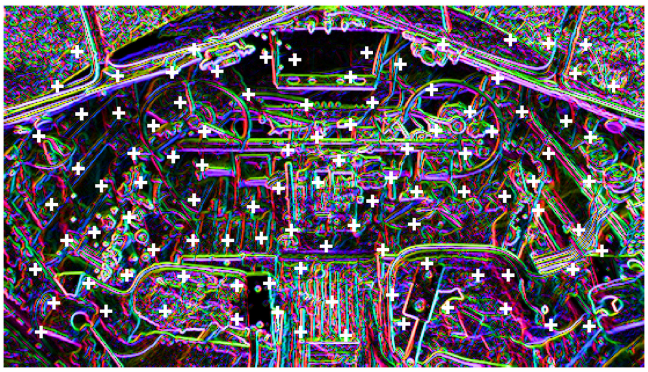

Fig. 8. Gradient field with 100 randomly selected templates used in a single run of the experiment. The colormap is the same as in Fig. 5.

The data used in this experiment come from a computer simulation, not from a real physical measurement. The simulation resulted in a 300-frame video, showing the time-development of the Kármán street.

In the initial frame, we selected a template with a typical vortex, see Fig. 9. Then we deformed the video by two different TAFTs, which comprised anisotropic scaling with a factor of 5/4 and 7/4, respectively. The task is to find all vortices of a similar shape modulo TAFT in each frame of the deformed video. The search is performed in the space of invariants Z_k. We search for all local minima of ℓ_2-distance below a user-defined threshold. Such a task definition is rather "soft", because it specifies neither the significance of the vortices to be detected nor the required degree of similarity with the template. The results may be controlled by the number/order of the invariants we use.[5]

We matched the template to each frame individually. We repeated the experiment for various maximum invariant order. So, we matched the templates in ten videos, which means we processed 3,000 frames altogether. The resulting videos showing the vortex tracking can be found at zoi.utia.cas.cz/Experiment-with-Karman-Street. Two sample frames, one for each deformation, can be seen in Fig. 10.

5. The number of matches may be influenced also by the choice of the threshold. To eliminate this influence, we used thresholds of the same significance in each moment order.

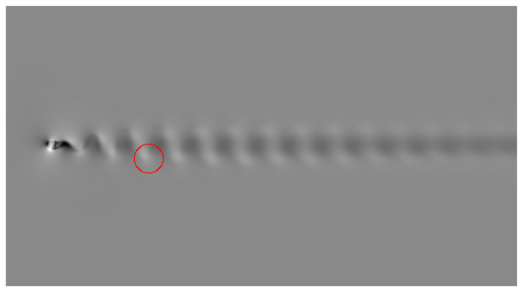

Fig. 9. The Kármán vortex street with the selected template (the first frame of the video).

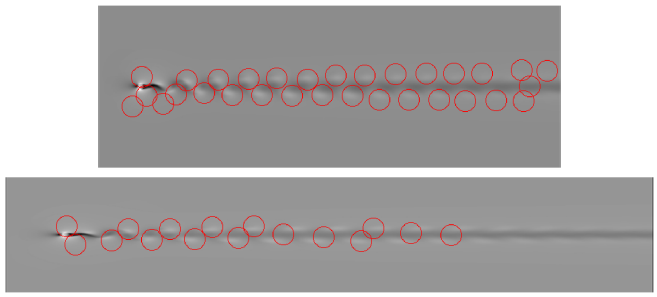

Fig. 10. The detected vortices in the deformed field when invariants Z_i up to 7th order were employed. The deformation comprised anisotropic scaling with factors 5/4 (top) and 7/4 (bottom). The full videos can be found at zoi.utia.cas.cz/Experiment-with-Karman-Street.

Since the ground truth is not known in this experiment, the matching accuracy cannot be evaluated quantitatively. However, visual inspection of the videos provide a good insight into the performance of the method. Most of the vortices were correctly found, but we can also observe some gross errors. They arose most probably because the neighborhood, the invariants were calculated from, was always circular and of the same size as the original template. To comply with all theoretical assumptions, the neighborhood should be transformed according to the inner transformation into an ellipse. However, we did not follow this approach in order to simulate real-world conditions (in practice, the transformation is unknown).

8.4 Vortex Detection in NOAA Data

In this experiment, we show on real data how our method can be used for vortex detection in weather satellite images and we also compare the results with two of "non-image" vortex detection methods [22]. We used the world wind maps from the NOAA satellite [46], which are publicly available through www.esrl.noaa.gov/psd/. We used 18 frames from different days. We extracted three typical circular templates of a wind vortex of the same size (two from the northern and one from the southern hemisphere). Then we tried to locate vortices of the same shape in the other frames. The results achieved by the invariants in two sample frames are shown in Fig. 11. For the template matching, we used 35 independent invariants up to the order five (both types V_i and Z_i were included). Since there is no measurable ground truth, we are left to a visual evaluation. We can see the detection

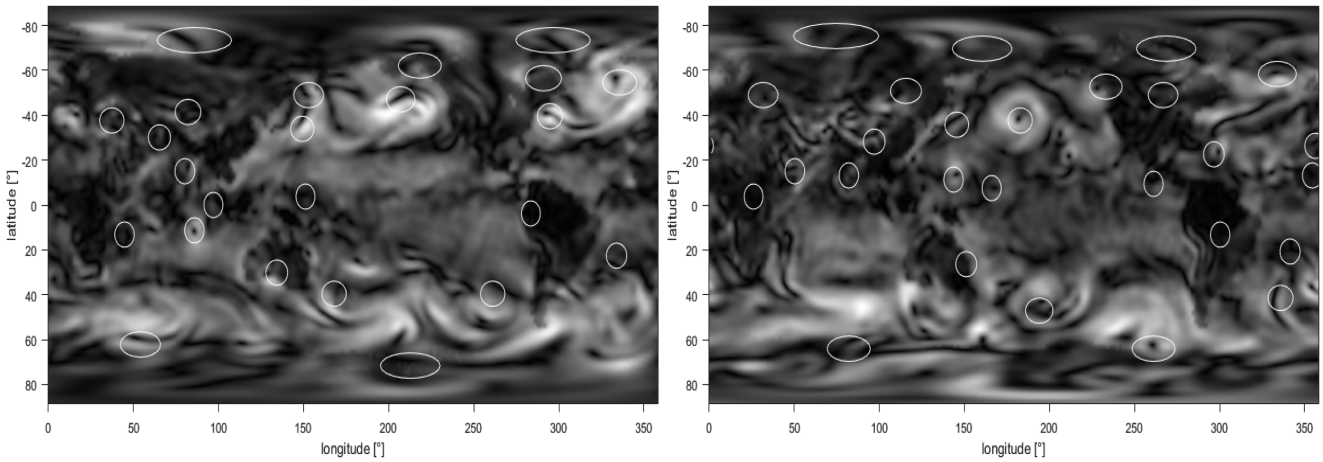

Fig. 11. Vortex detection in NOAA images by means of the invariants. The images display the wind magnitude only but the orientation is available as well and was used for the detection.

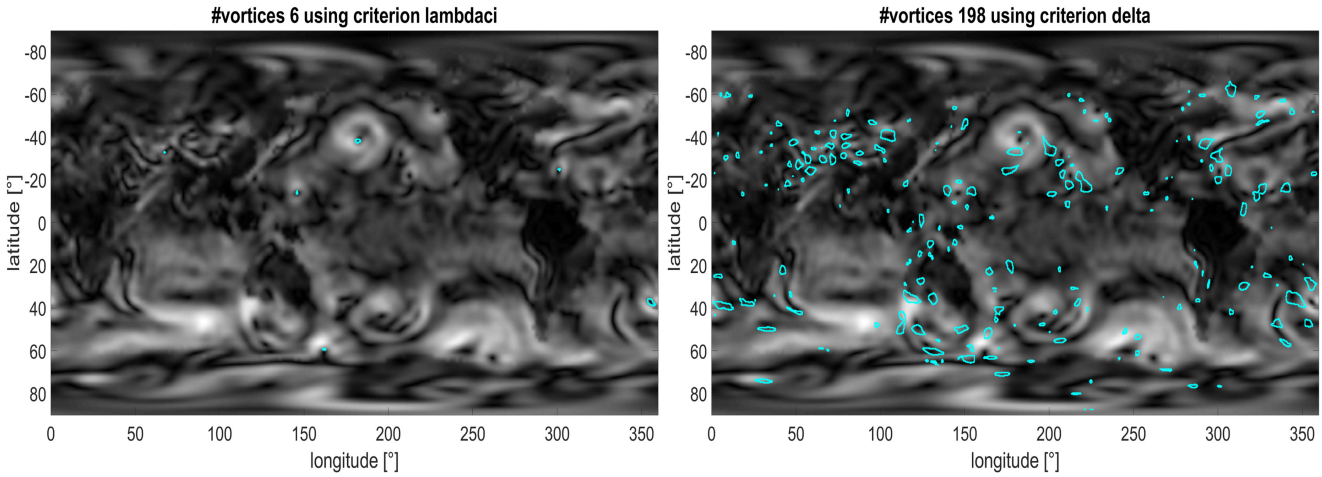

Fig. 12. Vortex detection by λ_{ci} (left) and Delta method (right) from [22]. The first method missed many vortices, the second one exhibits numerous false positives.

works quite well. Thanks to the affine invariance, also some vortices that exhibit an elongated shape due to data resampling in polar areas were detected (when searching the polar areas, the templates were not resampled, only the underlaying patch in the image was taken elliptical rather than circular). The method missed some vortices which look similar to the templates in magnitudes but their structure is different.

Then we applied the method from [22], which is a typical representative of "non-image" methods. It calculates the vorticity measure locally in each pixel from the gradient of the wind velocity. A vortex is a connected region where the vorticity measure exceeds a given threshold. We used two vorticity measures proposed in [22] – λ_{ci} and Delta criterion, respectively. The results for one frame are shown in Fig. 12. We can see that the sensitivity of the λ_{ci} method is low and only few vortices were found. On the other hand, the Delta method has higher sensitivity but low specificity, which leads to many false positives (as soon as the wind trajectory is curved enough, the area is considered to be a vortex). Both algorithms were applied with the parameter setting recommended in [22].

9 Conclusion

This paper introduced invariants of vector fields w.r.t. total affine transformation based on the moments of the vector field. The behavior of VFs under TAFT is significantly different from scalar and color images under standard affine transformation and the traditional techniques cannot be used. We derived new invariants in explicit closed form and showed that they can be represented by multilayer graphs. We also proposed the algorithm for selection of a maximal independent set of the invariants and use it to derive irreducible and independent invariants up to the weight nine. We demonstrated the performance of the invariants in template matching on gradient fields, on simulated data from fluid dynamics, and on real data from NOAA satellite. The comparison to rotation invariants and two "non-image" vortex detection methods showed the advantages of the proposed affine invariants.

Appendix A

Let $B = (B_{mn})$ be a regular outer transformation matrix. Then

$$
\begin{aligned}
F'_{kj} &= f'_1(x_k, y_k) f'_2(x_j, y_j) - f'_1(x_j, y_j) f'_2(x_k, y_k) \\
&= [B_{11} f_1(x_k, y_k) + B_{12} f_2(x_k, y_k)]\big[B_{21} f_1(x_j, y_j) \\
&\quad + B_{22} f_2(x_j, y_j)\big] - \big[B_{11} f_1(x_j, y_j) + B_{12} f_2(x_j, y_j)\big] \\
&\quad [B_{21} f_1(x_k, y_k) + B_{22} f_2(x_k, y_k)] \\
&= B_{11} B_{21} f_1(x_j, y_j) f_1(x_k, y_k) \\
&\quad + B_{11} B_{22} f_1(x_k, y_k) f_2(x_j, y_j) \\
&\quad + B_{12} B_{21} f_2(x_k, y_k) f_1(x_j, y_j) \\
&\quad + B_{12} B_{22} f_2(x_k, y_k) f_2(x_j, y_j) \\
&\quad - B_{11} B_{21} f_1(x_j, y_j) f_1(x_k, y_k) \\
&\quad - B_{11} B_{22} f_1(x_j, y_j) f_2(x_k, y_k) \\
&\quad - B_{12} B_{21} f_2(x_j, y_j) f_1(x_k, y_k) \\
&\quad - B_{12} B_{22} f_2(x_j, y_j) f_2(x_k, y_k) \\
&= (B_{11} B_{22} - B_{12} B_{21})\big[f_1(x_k, y_k) f_2(x_j, y_j) \\
&\quad - f_2(x_k, y_k) f_1(x_j, y_j)\big] = J_B \cdot F_{kj}\,.
\end{aligned}
$$

APPENDIX B

Let $A = (A_{mn})$ be a regular outer and inner transformation matrix. Then

$$
\begin{aligned}
D'_{kj} &= y'_j f'_1(x'_k, y'_k) - x'_j f'_2(x'_k, y'_k) \\
&= (A_{21} x_j + A_{22} y_j)[A_{11} f_1(x_k, y_k) + A_{12} f_2(x_k, y_k)] \\
&\quad - (A_{11} x_j + A_{12} y_j)[A_{21} f_1(x_k, y_k) + A_{22} f_2(x_k, y_k)] \\
&= A_{21} A_{11} x_j f_1(x_k, y_k) + A_{21} A_{12} x_j f_2(x_k, y_k) \\
&\quad + A_{22} A_{11} y_j f_1(x_k, y_k) + A_{22} A_{12} y_j f_2(x_k, y_k) \\
&\quad - A_{11} A_{21} x_j f_1(x_k, y_k) - A_{11} A_{22} x_j f_2(x_k, y_k) \\
&\quad - A_{12} A_{21} y_j f_1(x_k, y_k) - A_{12} A_{22} y_j f_2(x_k, y_k) \\
&= (A_{11} A_{22} - A_{12} A_{21})\big[y_j f_1(x_k, y_k) - x_j f_2(x_k, y_k)\big] \\
&= J_A \cdot D_{kj}\,.
\end{aligned}
$$

APPENDIX C

In this appendix, we present the multilayer graphs representing the invariants $V(\mathbf{f})$ (11). The black edges belong to E_1 and the magenta edges belong to E_2. The invariants $V_1, V_2, \ldots, V_8$ shown here were selected from the set of the irreducible invariants http://zoi.utia.cas.cz/affine-vector-fields, where they are labeled as $V_{r1}, V_{r2}, V_{r4}, V_{r7}, V_{r15}, V_{r18}, V_{r3}$, and V_{r19} respectively. The invariants $V_1, V_2, \ldots, V_8$ create a complete and independent set of the second and third-order VFAMIs. The invariants V_1 and V_2 are shown also in their explicit forms. For explicit formulas of all other invariants, please visit the website http://zoi.utia.cas.cz/affine-vector-fields.

$$
\begin{aligned}
V_1 &= -(\mu^{(1)}_{20})^2(\mu^{(2)}_{02})^2 + 4\mu^{(1)}_{20}\mu^{(1)}_{11}\mu^{(2)}_{11}\mu^{(2)}_{02} \\
&\quad + 2\mu^{(1)}_{20}\mu^{(1)}_{02}\mu^{(2)}_{20}\mu^{(2)}_{02} - 4\mu^{(1)}_{20}\mu^{(1)}_{02}(\mu^{(2)}_{11})^2 \\
&\quad - 4(\mu^{(1)}_{11})^2\mu^{(2)}_{20}\mu^{(2)}_{02} + 4\mu^{(1)}_{11}\mu^{(1)}_{02}\mu^{(2)}_{20}\mu^{(2)}_{11} - (\mu^{(1)}_{02})^2(\mu^{(2)}_{20})^2
\end{aligned}
$$

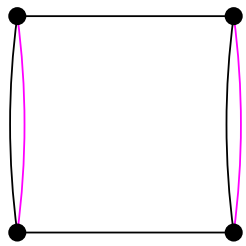

$$
V_2 = \mu^{(1)}_{30}\mu^{(2)}_{03} - 3\mu^{(1)}_{21}\mu^{(2)}_{12} + 3\mu^{(1)}_{12}\mu^{(2)}_{21} - \mu^{(1)}_{03}\mu^{(2)}_{30}
$$

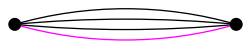

V_3

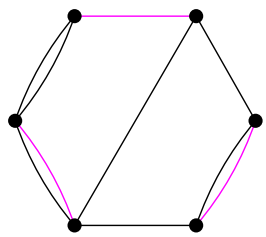

V_4

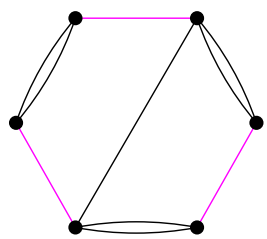

V_5

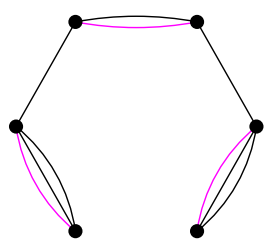

V_6

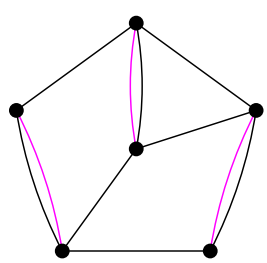

V_7

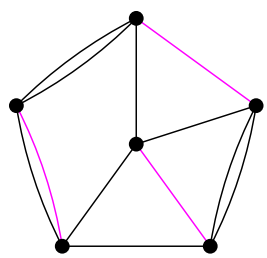

V_8

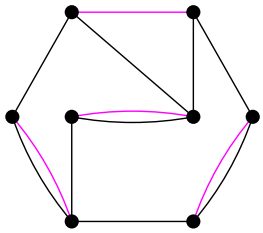

APPENDIX D

In this appendix, we present the multilayer graphs representing the invariants w.r.t. special total transformation $Z(\mathbf{f})$ (16). The black edges belong to E_1, the magenta edges belong to E_2, and the black-magenta edges depict the layer E_3 (the head-end of the edge is black). The invariants $Z_1, Z_2, \ldots, Z_{10}$ shown here were selected from the set of the irreducible invariants http://zoi.utia.cas.cz/affine-vector-fields, where they are labeled as $Z_{r3}, Z_{r4}, Z_{r6}, Z_{r8}, Z_{r9}, Z_{r19}, Z_{r20}, Z_{r21}, Z_{r11}$, and Z_{r13} respectively. The invariants $Z_1, Z_2, \ldots, Z_{10}$ create a complete and independent set of the second and third order. For higher-order invariants please visit the website http://zoi.utia.cas.cz/affine-vector-fields.

$$
\begin{aligned}
Z_1 = &-(\mu_{20}^{(1)})^2(\mu_{02}^{(2)})^2 + 4\mu_{20}^{(1)}\mu_{11}^{(1)}\mu_{11}^{(2)}\mu_{02}^{(2)} \\
&+ 2\mu_{20}^{(1)}\mu_{02}^{(1)}\mu_{20}^{(2)}\mu_{02}^{(2)} - 4\mu_{20}^{(1)}\mu_{02}^{(1)}(\mu_{11}^{(2)})^2 - 4(\mu_{11}^{(1)})^2\mu_{20}^{(2)}\mu_{02}^{(2)} \\
&+ 4\mu_{11}^{(1)}\mu_{02}^{(1)}\mu_{20}^{(2)}\mu_{11}^{(2)} - (\mu_{02}^{(1)})^2(\mu_{20}^{(2)})^2
\end{aligned}
$$

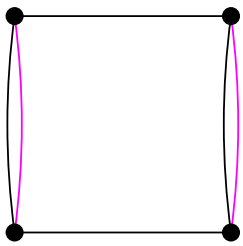

$$
\begin{aligned}
Z_2 = &\, 2\mu_{20}^{(1)}\mu_{20}^{(2)}\mu_{11}^{(2)}\mu_{02}^{(2)} - (\mu_{20}^{(1)})^2(\mu_{02}^{(2)})^2 - 2\mu_{20}^{(1)}(\mu_{11}^{(2)})^3 \\
&+ 2\mu_{20}^{(1)}\mu_{11}^{(1)}\mu_{11}^{(2)}\mu_{02}^{(2)} + 2\mu_{20}^{(1)}\mu_{11}^{(1)}\mu_{02}^{(1)}\mu_{02}^{(2)} - 2\mu_{20}^{(1)}(\mu_{02}^{(1)})^2\mu_{11}^{(2)} \\
&- 2\mu_{11}^{(1)}(\mu_{20}^{(2)})^2\mu_{02}^{(2)} + 2\mu_{11}^{(1)}\mu_{20}^{(2)}(\mu_{11}^{(2)})^2 - 2(\mu_{11}^{(1)})^3\mu_{02}^{(2)} \\
&+ 2(\mu_{11}^{(1)})^2\mu_{02}^{(1)}\mu_{11}^{(2)} - 2\mu_{11}^{(1)}\mu_{02}^{(1)}\mu_{20}^{(2)}\mu_{11}^{(2)} + (\mu_{02}^{(1)})^2(\mu_{20}^{(2)})^2
\end{aligned}
$$

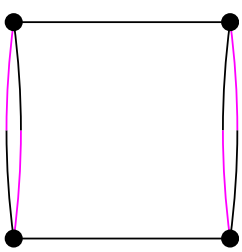

$$
\begin{aligned}
Z_3 = &\, (\mu_{20}^{(2)})^3\mu_{02}^{(2)} - (\mu_{20}^{(2)})^2(\mu_{11}^{(2)})^2 - \mu_{20}^{(1)}(\mu_{11}^{(2)})^3 \\
&+ 3\mu_{20}^{(1)}\mu_{02}^{(1)}(\mu_{11}^{(2)})^2 - 3\mu_{20}^{(1)}(\mu_{02}^{(1)})^2\mu_{11}^{(2)} + \mu_{20}^{(1)}(\mu_{02}^{(1)})^3 \\
&- 3\mu_{11}^{(1)}(\mu_{20}^{(2)})^2\mu_{02}^{(2)} + 5\mu_{11}^{(1)}\mu_{20}^{(2)}(\mu_{11}^{(2)})^2 + 3(\mu_{11}^{(1)})^2\mu_{20}^{(2)}\mu_{02}^{(2)} \\
&- 4(\mu_{11}^{(1)})^2(\mu_{11}^{(2)})^2 - (\mu_{11}^{(1)})^3\mu_{02}^{(2)} + 5(\mu_{11}^{(1)})^2\mu_{02}^{(1)}\mu_{11}^{(2)} \\
&- (\mu_{11}^{(1)})^2(\mu_{02}^{(1)})^2 - 4\mu_{11}^{(1)}\mu_{02}^{(1)}\mu_{20}^{(2)}\mu_{11}^{(2)} - \mu_{11}^{(1)}(\mu_{02}^{(1)})^2\mu_{20}^{(2)} \\
&- \mu_{02}^{(1)}(\mu_{20}^{(2)})^2\mu_{11}^{(2)} + 2(\mu_{02}^{(1)})^2(\mu_{20}^{(2)})^2
\end{aligned}
$$

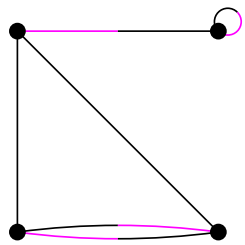

$$
Z_4 = \mu_{30}^{(1)}\mu_{03}^{(2)} - 3\mu_{21}^{(1)}\mu_{12}^{(2)} + 3\mu_{12}^{(1)}\mu_{21}^{(2)} - \mu_{03}^{(1)}\mu_{30}^{(2)}
$$

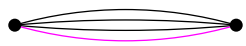

$$
\begin{aligned}
Z_5 = &-\mu_{30}^{(2)}\mu_{12}^{(2)} + \mu_{30}^{(1)}\mu_{03}^{(2)} + (\mu_{21}^{(2)})^2 - 2\mu_{21}^{(1)}\mu_{12}^{(2)} - \mu_{21}^{(1)}\mu_{03}^{(1)} \\
&+ \mu_{12}^{(1)}\mu_{21}^{(2)} + (\mu_{12}^{(1)})^2
\end{aligned}
$$

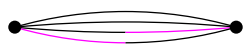

$$
\begin{aligned}
Z_6 = &-\mu_{20}^{(1)}\mu_{11}^{(2)}\mu_{12}^{(2)} - \mu_{20}^{(1)}\mu_{12}^{(1)}\mu_{02}^{(2)} + \mu_{20}^{(1)}\mu_{02}^{(2)}\mu_{21}^{(2)} \\
&+ \mu_{20}^{(1)}\mu_{03}^{(1)}\mu_{11}^{(2)} + \mu_{11}^{(1)}\mu_{20}^{(2)}\mu_{12}^{(2)} + \mu_{11}^{(1)}\mu_{21}^{(1)}\mu_{02}^{(2)} \\
&- \mu_{11}^{(1)}\mu_{02}^{(2)}\mu_{30}^{(2)} - \mu_{11}^{(1)}\mu_{03}^{(1)}\mu_{20}^{(2)} - \mu_{02}^{(1)}\mu_{20}^{(2)}\mu_{21}^{(2)} \\
&- \mu_{02}^{(1)}\mu_{21}^{(1)}\mu_{11}^{(2)} + \mu_{02}^{(1)}\mu_{11}^{(2)}\mu_{30}^{(2)} + \mu_{02}^{(1)}\mu_{12}^{(1)}\mu_{20}^{(2)}
\end{aligned}
$$

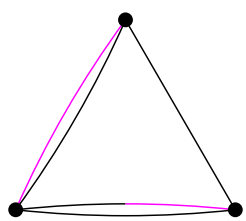

$$
\begin{aligned}
Z_7 = &\, \mu_{21}^{(1)}\mu_{20}^{(2)}\mu_{02}^{(2)} - \mu_{21}^{(1)}(\mu_{11}^{(2)})^2 - \mu_{20}^{(1)}\mu_{12}^{(1)}\mu_{02}^{(2)} \\
&- \mu_{20}^{(2)}\mu_{02}^{(2)}\mu_{30}^{(2)} + \mu_{20}^{(1)}\mu_{02}^{(2)}\mu_{21}^{(2)} - \mu_{20}^{(1)}\mu_{02}^{(1)}\mu_{12}^{(2)} \\
&+ \mu_{20}^{(1)}\mu_{02}^{(1)}\mu_{03}^{(1)} + (\mu_{11}^{(2)})^2\mu_{30}^{(2)} - 2\mu_{11}^{(1)}\mu_{11}^{(2)}\mu_{21}^{(2)} \\
&+ 2\mu_{11}^{(1)}\mu_{12}^{(1)}\mu_{11}^{(2)} + (\mu_{11}^{(1)})^2\mu_{12}^{(2)} - (\mu_{11}^{(1)})^2\mu_{03}^{(1)} \\
&+ \mu_{02}^{(1)}\mu_{20}^{(2)}\mu_{21}^{(2)} - \mu_{02}^{(1)}\mu_{12}^{(1)}\mu_{20}^{(2)}
\end{aligned}
$$

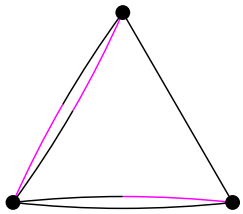

$$
\begin{aligned}
Z_8 = &-\mu_{30}^{(1)}\mu_{11}^{(2)}\mu_{02}^{(2)} + \mu_{21}^{(1)}\mu_{20}^{(2)}\mu_{02}^{(2)} - \mu_{20}^{(1)}\mu_{20}^{(2)}\mu_{03}^{(2)} \\
&+ 2\mu_{21}^{(1)}(\mu_{11}^{(2)})^2 + \mu_{20}^{(1)}\mu_{11}^{(2)}\mu_{12}^{(2)} + \mu_{20}^{(1)}\mu_{11}^{(1)}\mu_{03}^{(2)} \\
&- \mu_{20}^{(1)}\mu_{02}^{(1)}\mu_{12}^{(2)} - 3\mu_{12}^{(1)}\mu_{20}^{(2)}\mu_{11}^{(2)} + 2\mu_{11}^{(1)}\mu_{20}^{(2)}\mu_{12}^{(2)} \\
&- \mu_{11}^{(1)}\mu_{21}^{(1)}\mu_{02}^{(2)} - 2\mu_{11}^{(1)}\mu_{11}^{(2)}\mu_{21}^{(2)} + 2\mu_{11}^{(1)}\mu_{12}^{(1)}\mu_{11}^{(2)} \\
&- 2(\mu_{11}^{(1)})^2\mu_{12}^{(2)} - \mu_{11}^{(1)}\mu_{03}^{(1)}\mu_{20}^{(2)} + 3\mu_{11}^{(1)}\mu_{02}^{(1)}\mu_{21}^{(2)} \\
&+ \mu_{02}^{(1)}\mu_{30}^{(1)}\mu_{02}^{(2)} + \mu_{03}^{(1)}(\mu_{20}^{(2)})^2 - \mu_{02}^{(1)}\mu_{20}^{(2)}\mu_{21}^{(2)} \\
&- 2\mu_{02}^{(1)}\mu_{21}^{(1)}\mu_{11}^{(2)} + \mu_{02}^{(1)}\mu_{11}^{(2)}\mu_{30}^{(2)} + \mu_{02}^{(1)}\mu_{12}^{(1)}\mu_{20}^{(2)} \\
&- (\mu_{02}^{(1)})^2\mu_{30}^{(2)}
\end{aligned}
$$

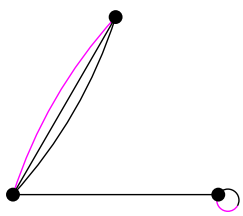

$$
\begin{aligned}
Z_9 = &\ \mu_{30}^{(1)}\mu_{21}^{(2)}\mu_{03}^{(2)} - \mu_{30}^{(1)}(\mu_{12}^{(2)})^2 + \mu_{30}^{(1)}\mu_{12}^{(1)}\mu_{03}^{(2)} \\
&- \mu_{30}^{(1)}\mu_{03}^{(1)}\mu_{12}^{(2)} - \mu_{21}^{(1)}\mu_{30}^{(2)}\mu_{03}^{(2)} + \mu_{21}^{(1)}\mu_{21}^{(2)}\mu_{12}^{(2)} - (\mu_{21}^{(1)})^2\mu_{03}^{(2)} \\
&+ \mu_{21}^{(1)}\mu_{12}^{(1)}\mu_{12}^{(2)} + \mu_{21}^{(1)}\mu_{03}^{(1)}\mu_{21}^{(2)} + \mu_{12}^{(1)}\mu_{30}^{(2)}\mu_{12}^{(2)} - \mu_{12}^{(1)}(\mu_{21}^{(2)})^2 \\
&- (\mu_{12}^{(1)})^2\mu_{21}^{(2)}
\end{aligned}
$$

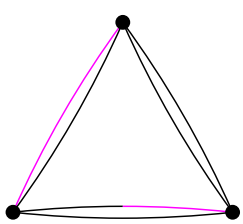

$$
\begin{aligned}
Z_{10} = &-(\mu_{30}^{(2)})^2\mu_{03}^{(2)} + 3\mu_{30}^{(2)}\mu_{21}^{(2)}\mu_{12}^{(2)} - \mu_{30}^{(1)}(\mu_{12}^{(2)})^2 \\
&+ 2\mu_{30}^{(1)}\mu_{03}^{(1)}\mu_{12}^{(2)} - \mu_{30}^{(1)}(\mu_{03}^{(1)})^2 + 2\mu_{21}^{(1)}\mu_{30}^{(2)}\mu_{03}^{(2)} \\
&- 2(\mu_{21}^{(2)})^3 + \mu_{21}^{(1)}\mu_{21}^{(2)}\mu_{12}^{(2)} - (\mu_{21}^{(1)})^2\mu_{03}^{(2)} + \mu_{21}^{(1)}\mu_{12}^{(1)}\mu_{12}^{(2)} \\
&+ 3\mu_{21}^{(1)}\mu_{12}^{(1)}\mu_{03}^{(1)} - 5\mu_{21}^{(1)}\mu_{03}^{(1)}\mu_{21}^{(2)} - 5\mu_{12}^{(1)}\mu_{30}^{(2)}\mu_{12}^{(2)} \\
&+ 2\mu_{12}^{(1)}(\mu_{21}^{(2)})^2 + 2(\mu_{12}^{(1)})^2\mu_{21}^{(2)} - 2(\mu_{12}^{(1)})^3 \\
&+ \mu_{12}^{(1)}\mu_{03}^{(1)}\mu_{30}^{(2)} + \mu_{03}^{(1)}\mu_{30}^{(2)}\mu_{21}^{(2)}
\end{aligned}
$$

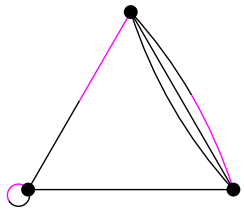

ACKNOWLEDGMENTS

This work has been supported by the Czech Science Foundation under the grant No. GA18-07247S, by the Grant SGS18/188/OHK4/3T/14 provided by the Ministry of Education, Youth, and Sports of the Czech Republic (MŠMT ČR), and by the *Praemium Academiae*. The authors would like to thank Prof. Mario Hlawitschka and Dr. Roxana Bujack for providing the Karman vortex street data, and the NOAA ESRL Physical Sciences Division, Boulder, Colorado, for providing the wind maps.

REFERENCES

[1] J. Flusser, T. Suk, and B. Zitová, *Moments and Moment Invariants in Pattern Recognition*. Chichester, U.K.: Wiley, 2009.
[2] J. Flusser, T. Suk, and B. Zitová, *2D and 3D Image Analysis by Moments*. Chichester, U.K.: Wiley, 2016.
[3] M. Schlemmer *et al.*, "Moment invariants for the analysis of 2D flow fields," *IEEE Trans. Vis. Comput. Graphics*, vol. 13, no. 6, pp. 1743–1750, Nov./Dec. 2007.
[4] Y. S. Abu-Mostafa and D. Psaltis, "Recognitive aspects of moment invariants," *IEEE Trans. Pattern Anal. Mach. Intell.*, vol. PAMI-6, no. 6, pp. 698–706, Nov. 1984.
[5] J. Flusser, "On the independence of rotation moment invariants," *Pattern Recognit.*, vol. 33, no. 9, pp. 1405–1410, 2000.
[6] J. Flusser, "On the inverse problem of rotation moment invariants," *Pattern Recognit.*, vol. 35, no. 12, pp. 3015–3017, 2002.
[7] W. Liu and E. Ribeiro, "Detecting singular patterns in 2-D vector fields using weighted Laurent polynomial," *Pattern Recognit.*, vol. 45, no. 11, pp. 3912–3925, 2012.
[8] M. Liu and P.-T. Yap, "Invariant representation of orientation fields for fingerprint indexing," *Pattern Recognit.*, vol. 45, no. 7, pp. 2532–2542, 2012.
[9] M. Langbein and H. Hagen, "A generalization of moment invariants on 2D vector fields to tensor fields of arbitrary order and dimension," in *Proc. 5th Int. Symp. Advances Vis. Comput.*, 2009, pp. 1151–1160.
[10] R. Bujack, I. Hotz, G. Scheuermann, and E. Hitzer, "Moment invariants for 2D flow fields using normalization," in *Proc. IEEE Pacific Vis. Symp.*, Mar. 2014, pp. 41–48.
[11] R. Bujack, M. Hlawitschka, G. Scheuermann, and E. Hitzer, "Customized TRS invariants for 2D vector fields via moment normalization," *Pattern Recognit. Lett.*, vol. 46, no. 1, pp. 46–59, 2014.
[12] B. Yang, J. Kostková, T. Suk, J. Flusser, and R. Bujack, "Recognition of patterns in vector fields by Gaussian–Hermite invariants," in *Proc. Int. Conf. Image Process.*, 2017, pp. 2350–2363.
[13] B. Yang, J. Kostková, J. Flusser, T. Suk, and R. Bujack, "Rotation invariants of vector fields from orthogonal moments," *Pattern Recognit.*, vol. 74, pp. 110–121, 2018.
[14] R. Bujack and J. Flusser, "Flexible basis of rotation moment invariants," in *Proc. Int. Conf. Central Eur. Comput. GraphicsVis. Comput. Vis.*, Pilsen, Czech Rep., May 2017, pp. 11–20.
[15] M. Jiang, R. Machiraju, and D. Thompson, "Detection and visualization of vortices," *Visualization Handbook*, C. D. Hansen, and C. R. Johnson, Eds. Elsevier, 2011.
[16] D. Degani, A. Seginer, and Y. Levy, "Graphical visualization of vortical flows by means of helicity," *AIAA J.*, vol. 28, no. 8, pp. 1347–1352, 1990.
[17] C. Berdahl and D. Thompson, "Eduction of swirling structure using the velocity gradient tensor," *AIAA J.*, vol. 31, no. 1, pp. 97–103, 1993.

[18] J. Jeong and F. Hussain, "On the identification of a vortex," *J. Fluid Mech.*, vol. 285, pp. 69–94, 1995.
[19] D. C. Banks and B. A. Singer, "A predictor-corrector technique for visualizing unsteady flow," *IEEE Trans. Vis. Comput. Graphics*, vol. 1, no. 2, pp. 151–163, Jun. 1995.
[20] M. Roth and R. Peikert, "A higher-order method for finding vortex core lines," in *Proc. Vis. (Cat. No. 98CB36276)*, 1998, pp. 143–150.
[21] I. A. Sadarjoen, F. H. Post, B. Ma, D. C. Banks, and H.-G. Pagendarm, "Selective visualization of vortices in hydrodynamic flows," in *Proc. Vis. (Cat. No. 98CB36276)*, 1998, pp. 419–422.
[22] Q. Chen, Q. Zhong, M. Qi, and X. Wang, "Comparison of vortex identification criteria for planar velocity fields in wall turbulence," *Phys. Fluids*, vol. 27, no. 8, 2015, Art. no. 085101.
[23] D. Hilbert, *Theory of Algebraic Invariants*. Cambridge, U.K.: Cambridge Univ. Press, 1993.
[24] J. H. Grace and A. Young, *The Algebra of Invariants*. Cambridge, U.K.: Cambridge Univ. Press, 1903.
[25] J. J. Sylvester, "Tables of the generating functions and groundforms for the binary quantics of the first ten orders," *Amer. J. Math.*, vol. 2, pp. 223–251, 1879.
[26] J. J. Sylvester, "Tables of the generating functions and groundforms for simultaneous binary quantics of the first four orders taken two and two together," *Amer. J. Math.*, vol. 2, pp. 293–306, 324–329, 1879.
[27] I. Schur, *Vorlesungen über Invariantentheorie*. Berlin, Germany: Springer, 1968.
[28] G. B. Gurevich, *Foundations of the Theory of Algebraic Invariants*. Groningen, The Netherlands: Nordhoff, 1964.
[29] M.-K. Hu, "Visual pattern recognition by moment invariants," *IRE Trans. Inf. Theory*, vol. 8, no. 2, pp. 179–187, 1962.
[30] T. H. Reiss, "The revised fundamental theorem of moment invariants," *IEEE Trans. Pattern Anal. Mach. Intell.*, vol. 13, no. 8, pp. 830–834, Aug. 1991.
[31] J. Flusser and T. Suk, "Pattern recognition by affine moment invariants," *Pattern Recognit.*, vol. 26, no. 1, pp. 167–174, 1993.
[32] T. Suk and J. Flusser, "Graph method for generating affine moment invariants," in *Proc. 17th Int. Conf. Pattern Recognit.*, 2004, pp. 192–195.
[33] T. Suk and J. Flusser, "Affine moment invariants generated by graph method," *Pattern Recognit.*, vol. 44, no. 9, pp. 2047–2056, 2011.
[34] T. H. Reiss, *Recognizing Planar Objects Using Invariant Image Features*. Berlin, Germany: Springer, 1993.
[35] T. Suk and J. Flusser, "Affine moment invariants generated by automated solution of the equations," in *Proc. 19th Int. Conf. Pattern Recognit.*, 2008, pp. 1–4.
[36] M. S. Hickman, "Geometric moments and their invariants," *J. Math. Imag. Vis.*, vol. 44, no. 3, pp. 223–235, 2012.
[37] I. Rothe, H. Süsse, and K. Voss, "The method of normalization to determine invariants," *IEEE Trans. Pattern Anal. Mach. Intell.*, vol. 18, no. 4, pp. 366–376, Apr. 1996.
[38] T. Suk and J. Flusser, "Affine moment invariants of color images," in *Proc. Int. Conf. Comput. Anal. Images Patterns*, Springer, Sep. 2009, vol. LNCS 5702, pp. 334–341.
[39] F. Mindru, T. Moons, and L. V. Gool, "Color-based moment invariants for viewpoint and illumination independent recognition of planar color patterns," in *Proc. Int. Conf. Advances Pattern Recognit.*, 1998, pp. 113–122.
[40] F. Mindru, T. Tuytelaars, L. V. Gool, and T. Moons, "Moment invariants for recognition under changing viewpoint and illumination," *Comput. Vis. Image Understanding*, vol. 94, no. 1–3, pp. 3–27, 2004.
[41] M. Gong, Y. Hao, H. Mo, and H. Li, "Naturally combined shape-color moment invariants under affine transformations," *Comput. Vis. Image Understanding*, vol. 162, pp. 46–56, 2017.
[42] J. Kostková and J. Flusser, "On the null-space of the shape-color moment invariants," in *Proc. Int. Conf. Comput. Anal. Images Patterns*, Springer, 2019, vol. LNCS 11678, pp. 402–408.
[43] G. Finlayson, M. Drew, and B. Funt, "Color constancy: Generalized diagonal transforms suffice," *J. Opt. Soc. America A*, vol. 11, no. 11, pp. 3011–3019, 1994.
[44] T. Gevers and A. Smeulders, "A comparative study of several color models for color image invariant retrieval," in *Proc. 1st Int. Workshop Image Database Multimedia Search*, 1996, pp. 17–23.
[45] A. B. Brown, "Functional dependence," *Trans. Amer. Math. Soc.*, vol. 38, no. 2, pp. 379–394, 1935.
[46] E. Kalnay *et al.*, "The NCEP/NCAR 40-year reanalysis project," *Bull. Amer. Meteorological Soc.*, vol. 77, no. 3, pp. 437–472, 1996.

Jitka Kostková received the MSc degree in applied mathematical stochastic methods from the Faculty of Nuclear Science and Physical Engineering, Czech Technical University, Prague, Czech Republic, in 2015. Currently, she is working toward the PhD degree in mathematical engineering and tutors undergraduate courses on mathematical analysis at the Czech Technical University. Her research interest include focused on moments and moment invariants.

Tomáš Suk received the MSc degree in electrical engineering from the Faculty of Electrical Engineering, Czech Technical University, Prague, Czech Republic, in 1987, the PhD degree in computer science from the Czechoslovak Academy of Sciences, in 1992, and the DSc degree from the Czech Academy of Sciences, in 2018. Since 1991, he has been a researcher with the Institute of Information Theory and Automation, Czech Academy of Sciences, Prague. He has authored more than 35 journal papers, more than 50 conference papers and coauthored the *Monographs Moments and Moment Invariants in Pattern Recognition* (Wiley, 2009) and *2D and 3D Image Analysis by Moments* (Wiley, 2016). His research interests include digital image processing, pattern recognition, image filtering, invariant features, moment-based and point-based invariants, spatial transformations of images, and applications in remote sensing, astronomy, botany, medicine, and computer vision. In 2002, he received the Otto Wichterle Premium of the Czech Academy of Sciences for excellent young scientists.

Jan Flusser received the MSc degree in mathematical engineering from the Czech Technical University, Prague, Czech Republic, in 1985, the PhD degree in computer science from the Czechoslovak Academy of Sciences, in 1990, and the DrSc degree in technical cybernetics, in 2001. Since 1985, he has been with the Institute of Information Theory and Automation, Czech Academy of Sciences, Prague. In 1995–2007, he was holding the position of a head of the Department of Image Processing. Since 2007, he has been a director of the Institute. He is a full professor of computer science with the Czech Technical University, Faculty of Nuclear Science and Physical Engineering, and with the Charles University, Faculty of Mathematics and Physics, Prague, where he gives undergraduate and graduate courses on digital image processing, pattern recognition, and moment invariants and wavelets. His research interest covers moments and moment invariants, image registration, image fusion, multichannel blind deconvolution, and super-resolution imaging. He has authored and coauthored more than 200 research publications in these areas, including the *Monographs Moments and Moment Invariants in Pattern Recognition* (Wiley, 2009) and *2D and 3D Image Analysis by Moments* (Wiley, 2016). In 2007, he received the Award of the Chairman of the Czech Science Foundation for the best research project and won the prize of the Academy of Sciences of the Czech Republic for the contribution to image fusion theory. In 2010, he was awarded by the SCOPUS 1000 Award. He received the Felber Medal of the Czech Technical University for excellent contribution to research and education in 2015 and the Praemium Academiae of the Czech Academy of Sciences for outstanding researchers in 2017. He is a senior member of the IEEE.